Deep-Sea Research II 118 (2015) 105–121

Contents lists available at ScienceDirect

Deep-Sea Research II

journal homepage: www.elsevier.com/locate/dsr2

Impacts of low phytoplankton NO_3^-:PO_4^{3-} utilization ratios over the Chukchi Shelf, Arctic Ocean

Matthew M. Mills [a,*], Zachary W. Brown [a], Kate E. Lowry [a], Gert L. van Dijken [a], Susan Becker [b], Sharmila Pal [c], Claudia R. Benitez-Nelson [c], Meryssa M. Downer [c], Aaron L. Strong [d], James H. Swift [b], Robert S. Pickart [e], Kevin R. Arrigo [a]

[a] Department of Environmental Earth System Science, Stanford University, Stanford, CA 94305, USA
[b] Scripps Institution of Oceanography, University of California San Diego, La Jolla, CA 92093, USA
[c] Marine Science Program & Department of Earth and Ocean Sciences, University of South Carolina, Columbia, SC 29208, USA
[d] Emmett Interdisciplinary Program in Environment and Resources, Stanford University, Stanford, CA 94305, USA
[e] Department of Physical Oceanography, Woods Hole Oceanographic Institution, Woods Hole, MA 02543, USA

ARTICLE INFO

Available online 7 February 2015

Keywords:
Phytoplankton
Chukchi
N:P ratio
N**
Non-Redfield
Denitrification

ABSTRACT

The impact of Arctic denitrification is seen in the extremely low values for the geochemical tracer of microbial nitrogen (N) cycle source/sink processes N^{**} (Mordy et al. 2010). The utility of N^{**} as an oceanic tracer of microbial N cycle processes, however, relies on the assumption that phytoplankton utilize dissolved N and P in Redfield proportions, and thus changes in N^{**} are due to either N_2-fixation or denitrification. We present results from two cruises to the Chukchi Sea that quantify nutrient drawdown, nutrient deficits, and particulate nutrient concentrations to estimate production over the Chukchi Shelf and document lower than Redfield N:P utilization ratios by phytoplankton. These low ratios are used to calculate N^{**} (assuming a Redfield NO_3^-:PO_4^{3-} utilization ratio) and N^{**}_{NR} (using the measured particulate N:P ratios) and, combined with current flow speed and direction measurements, to diagnose denitrification rates on the Chukchi Shelf. Our estimates of denitrification rates are up to 40% higher when Redfield proportions are used. However, the denitrification rates we calculate using N^{**}_{NR} are still higher than previous estimates (up to 8 fold) of denitrification on the Chukchi shelf. These estimates suggest that Arctic shelves may be a greater sink of oceanic N than previously thought.

1. Introduction

The Arctic Ocean is the world's smallest ocean but contains 20% of its continental shelves. Despite its relatively small size, the Arctic Ocean plays a major role in global ocean biogeochemistry, particularly with respect to the nitrogen (N) cycle. Given the large area of continental shelf in the Arctic Ocean, and that the shelf waters have relatively high productivity (Arrigo and Van Dijken, 2011), the Arctic Ocean is an important locus of denitification. Significant rates of sediment denitrification have been measured in the Arctic ($\sim$13 Tg N yr^{-1}), accounting for 4–13% of global marine denitrification (Devol et al., 1997; Chang and Devol, 2009). These high rates condition the water as it flows from the Pacific Ocean, through the Arctic, and into the Atlantic such that it has low dissolved inorganic N relative to dissolved inorganic phosphorus (P). This input of relatively P-rich water is believed to be a major source of P for N-fixing organisms in the oligotrophic North Atlantic (Yamamoto-Kawai et al., 2006).

Sediment denitrification is linked to water column productivity through the export of particulate organic matter that is subsequently oxidized by microbial denitrifiers using nitrate (NO_3^-) as the electron acceptor (Ward, 2013). Primary production in the Arctic Ocean varies regionally depending, in part, on the extent and persistence of sea ice (Arrigo and Van Dijken, 2011). The Greenland and Barents Seas typically have the largest open water area and are the most productive seas (Pabi et al., 2008). However, summer sea ice extent is decreasing rapidly, particularly in the Pacific sector of the Arctic Ocean. Those regions experiencing the largest losses of sea ice also have corresponding increases in annual net primary production (NPP) (Arrigo and Van Dijken, 2011). For example, in the Chukchi Sea, the number of open water days increased by 4.5 days per year between 1998 and 2009, while annual NPP increased by 48% (Arrigo and Van Dijken, 2011). In

* Corresponding author.

http://dx.doi.org/10.1016/j.dsr2.2015.02.007
0967-0645/

contrast, the Greenland Sea has experienced little change in sea ice and annual NPP declined by 2% between 1998 and 2009 (Arrigo and Van Dijken, 2011).

The relationship between denitrification and primary productivity suggests that denitrification likely varies regionally within the Arctic, with regions of highest NPP (Greenland and Barents Seas) expected to have the highest rates of denitrification. However, Chang and Devol (2009) argue that, while the Barents Sea does have high total annual rates of denitrification, rates are relatively low in the Greenland Sea. In contrast, the Chukchi Sea, which has a total annual rate of primary production 20–50% of that measured in the Greenland Sea (Sakshaug, 2004; Arrigo and Van Dijken, 2011), has a total annual sediment denitrification rate that is 1–2 orders of magnitude greater than estimated for the Greenland Sea, and is on par with that estimated in the Barents Sea (Chang and Devol, 2009). Thus, other factors besides production, such as O_2 concentration, water column depth, and advection, are likely important in determining rates of sediment denitrification.

The utilization and remineralization of nutrients by marine phytoplankton and bacteria alter oceanic nutrient inventories in predictable ways (Gruber, 2008). Geochemists measuring changes in nutrient ratios can often infer these biological processes without directly measuring them. For example, NO_3^- and phosphate (PO_4^{3-}) concentrations co-vary throughout the deep ocean in a ratio of ~14.7:1 (Redfield, 1958; Gruber and Sarmiento, 1997), close to the average N:P ratio of phytoplankton (Klausmeier et al., 2004). Deviations from this stoichiometry have been used to estimate the microbial processes of N fixation (N source) and denitrification (N sink), which change the ratio of the dissolved N and P pools differently than phytoplankton utilization (Gruber and Sarmiento, 1997). The biogeochemical nutrient tracer N^* (Deutsch et al., 2001; Gruber and Sarmiento, 1997) is primarily used in this manner and is calculated as

$$N^* = \left([DIN] - r_{N:P} \times \left[PO_4^{3-}\right]\right) + 2.9, \quad (1)$$

where $[DIN]$ equals the sum of NO_3^-, nitrite (NO_2^-), and ammonium (NH_4^+), and $r_{N:P}$ equals the Redfield N:P ratio of 16:1.

The utility of N^* as an oceanic tracer of microbial N cycle processes relies on the assumption that phytoplankton utilize dissolved N and P in Redfield proportions, and thus any deviations from the Redfield ratio are inferred as being due to either N-fixation or denitrification. This assumption, while representative of the global ocean nutrient utilization ratio for phytoplankton, does not hold across all taxa or all growth conditions. There is ample evidence that the N:P content of phytoplankton cells is related to evolutionary history, as well as growth strategy (Quigg et al., 2003, 2011). For example, different superfamiles of phytoplankton have different N:P ratios, with the green superfamily exhibiting greater than Redfield proportions (N:P ≈ 27), while the red superfamily has a N:P ratio below Redfield (N:P ≈ 10) (Quigg et al., 2003). These differences have been attributed to the phenotypes of the pre-ancestral symbiotic hosts from which these different superfamilies evolved.

The preponderance of non-Redfield stoichiometry among phytoplankton means that the standard calculation of geochemical tracers like N^*, which is based on Redfield stoichiometry, can be misleading. For example, Mills and Arrigo (2010) showed that rates of N-fixation in the eastern tropical South Pacific Ocean inferred from NO_3^- and PO_4^{3-} inventories are four-fold too high when non-Redfield N:P stoichiometry of phytoplankton is ignored.

In the Chukchi Sea, the NO_3^-:PO_4^{3-} ratio is lower than Redfield proportions (Kaltin and Anderson, 2005; Codispoti et al., 2013). This low ratio is typically ascribed to the high rates of sediment denitrification (Devol et al., 1997; Chang and Devol, 2009); however, low N:P utilization by phytoplankton would result in geochemical underestimates of denitrification where Redfield stoichiometry is assumed. The goal of the present study is to determine the impact of non-Redfield nutrient utilization by phytoplankton on excess N concentrations and geochemical estimates of denitrification in the Chukchi Sea. During cruises in the summers of 2010 and 2011, we measured ratios of nutrient utilization, particulate N and P, and nutrient deficits to document the extent of phytoplankton non-Redfield nutrient consumption during the phytoplankton growing season. We then calculated N^{**}, a modified version of N^* (see Mordy et al., 2010), using both Redfield stoichiometry and our empirically determined nutrient utilization ratios (N^{**}_{NR}). Finally, changes in N^{**} and N^{**}_{NR} along the Pacific water flow path in the central Chukchi Sea were used to estimate the degree to which phytoplankton non-Redfield nutrient utilization affect estimates of denitrification on the Chukchi Shelf.

2. Methods

2.1. Study site

The flow of water in the Chukchi Sea is to first order dictated by the bathymetry of the shelf (e.g., Weingartner et al., 2005; Spall, 2007). Three main pathways emanate northward from Bering Strait (Fig. 1): a western branch that goes through Herald Canyon; a middle branch that progresses through Central Channel (the gap between Herald Shoal and Hanna Shoal); and an eastern branch that flows adjacent to the coast of Alaska. In summertime, the eastern branch is known as the Alaskan Coastal Current (ACC), which transports warm and fresh Alaskan Coastal Water (ACW) originating from coastal runoff in the Gulf of Alaska and Bering Sea. The middle branch is believed to transport a combination of Bering Shelf Water and Anadyr Water (AW), which ultimately mix to form Bering Seawater (BSW). The western branch is thought to advect primarily AW. The ACC is typically warm (>2 °C) and depleted in nutrients (Fig. 2), with a significant

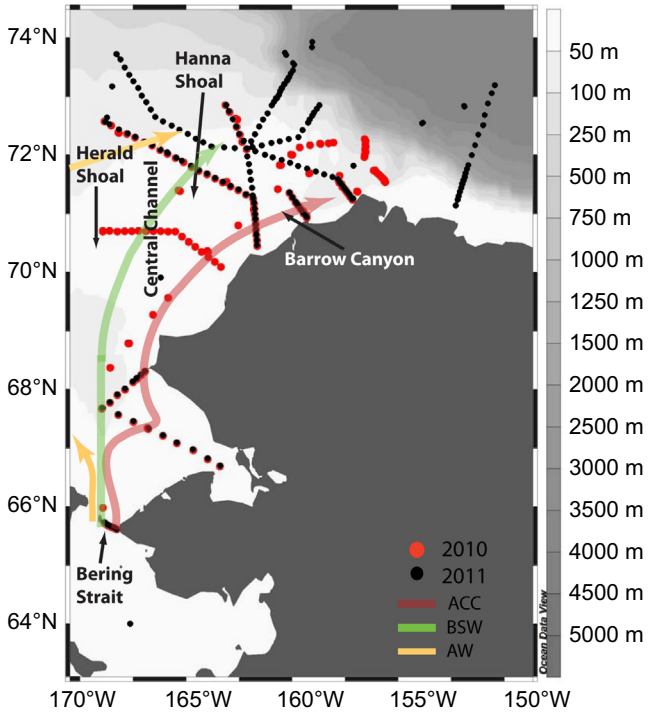

Fig. 1. Map of the stations sampled in the Chukchi Sea during 2010 (red) and 2011 (black) ICESCAPE cruises. Shown are the pathways of flow for the Alaskan Coastal Current (ACC), the Bering Seawater (BSW), and Anadyr Water (AW). (For interpretation of the references to color in this figure legend, the reader is referred to the web version of this article.)

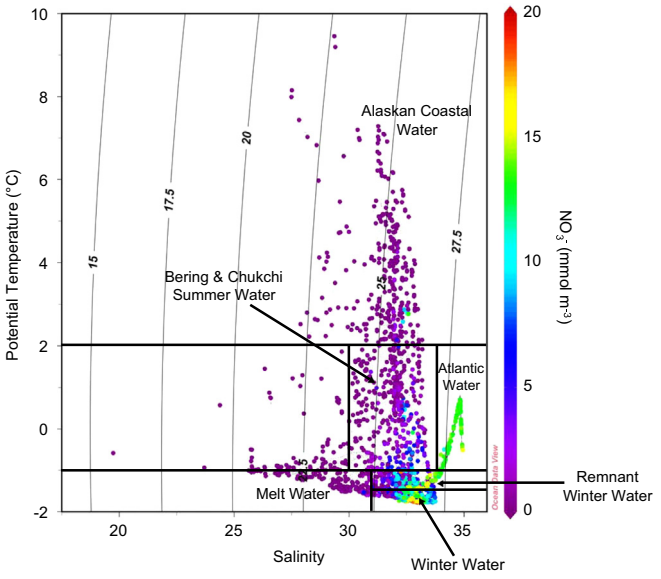

Fig. 2. Potential temperature (°C) vs. salinity plot showing the different water masses on the Chukchi Shelf observed during ICESCAPE in 2011 and 2012. Colors indicate NO^{3-} concentration (mmol m^{-3}). (For interpretation of the references to color in this figure legend, the reader is referred to the web version of this article.)

contribution from river input. In contrast, the summertime BSW is generally colder (−1 to 2 °C) than the ACW and has higher nutrient concentrations (Fig. 2). Some fraction of the AW in the western flow branch is diverted eastward toward the BSW (e.g., Pickart et al., 2010) and the combined flow is then steered around Hanna Shoal towards Barrow Canyon (Fig. 1). As such, all three Pacific water masses can, to some extent, exit the Chukchi Sea through Barrow Canyon.

In early winter, ice formation and brine rejection over the Chukchi shelf drives convective overturning that mixes the water column. As winter progresses, the whole of the Chukchi Sea becomes ice covered, daylight disappears, and inorganic nutrient concentrations increase due to microbial net remineralization of organic matter. The combination of the brine-induced mixing and nutrient regeneration results in a fully-mixed, nutrient-rich water column that persists until ice melt begins in the spring, when light levels are high enough for phytoplankton to start drawing down nutrients and begin fixing carbon. Sea ice retreat in the Chukchi Sea starts in the south and progresses northward through the late spring and early summer, facilitating the development of open water phytoplankton blooms. In recent years, thinner ice with high melt pond fractions has increased light penetration into the water below, allowing phytoplankton to consume nutrients even though ice is still present (Arrigo et al., 2012).

2.2. Sample collection

The eastern Chukchi Sea (Fig. 1) was sampled during two summer cruises aboard the USCGC *Healy* as a part of the Impacts of Climate on Ecosystems and Chemistry of the Arctic Pacific Environment (ICESCAPE) field campaign. Additionally, during the 2011 cruise, we also sampled the western Beaufort Sea, Arctic Ocean. The first cruise took place from June 15–July 21, 2010, and the second cruise from June 25–July 29, 2011. Sampling consisted of regularly spaced stations (135 stations in 2010 and 173 stations in 2011) along transects throughout the study region. At each station, a rosette equipped with 12 30 L Niskin bottles and conductivity–temperature–depth sensors (CTD, SBE 911+, Sea-bird Electronics, Inc.) was lowered to just above the seafloor to obtain vertical profiles of physical, chemical, and biological parameters. Measurement accuracies are estimated to be 0.008 °C for temperature and 0.004 for salinity for shelf waters, and 0.002 °C and 0.002, respectively, for deeper slope waters. Additional instruments attached to the CTD/rosette system included an oxygen (O_2) sensor (SBE43, Sea-bird Electronics, Inc.), two transmissometers (C-Star red and blue, WET labs), a photosynthetically active radiation (PAR) sensor (QSP2300 PAR, Biospherical Instruments, Inc.), and a fluorometer (AQIII, Chelsea Technologies Group, Ltd.).

Seawater velocity was measured using a hull mounted acoustic Doppler current profiler (ADCP, Ocean Surveyor 150 KHz, Teledyne RD Instruments). The data were acquired using the University of Hawaii's UHDAS software and underwent further processing with the CODAS3 software package (see http://currents.soest.hawaii.edu). The velocities (± 2 cm s^{-1}) were then de-tided using the Oregon State University model (http://volkov.oce.orst.edu/tides; Padman and Erofeeva, 2004). The accuracy of the resulting velocities is estimated to be ± 2 cm s^{-1}.

Seawater was collected at discrete depths using the Niskin bottles, typically just below the surface, 10, 25, 50, 100, 150, and 200 m, as well as at the depth of the chlorophyll *a* (Chl *a*) maximum (if present). An additional deep sample was collected ~2 m above the bottom. Once the rosette was onboard, the Niskin bottles were sampled for salinity, O_2, nutrients (NO_3^-, NO_2^-, NH_4^+, PO_4^{3-}, and silicate ($Si(OH)_4$)), Chl *a*, particulate organic carbon (POC), particulate organic N (PON), and different particulate P fractions (particulate organic P (POP), particulate inorganic P (PIP), and total particulate P (TPP)).

2.3. Analytical methods

Samples for fluorometric analysis of Chl *a* were filtered onto 25 mm Whatman GF/F filters (nominal pore size 0.7 μm) placed in 5 mL of 90% acetone, and extracted in the dark at 3 °C for 24 h. Chl *a* was measured fluorometrically (Holm-Hansen et al., 1965) using a Turner Fluorometer 10-AU (Turner Designs, Inc.) POC, PON, and POP samples were collected by filtering subsamples onto pre-combusted (450 °C for 4 h) 25 mm Whatman GF/F filters. The filters were then immediately dried at 60 °C and stored dry until processing. POP filters were also pre-rinsed with 10% hydrochloric acid (HCl). Prior to analysis for POC and PON, the samples were fumed in a dessicator with concentrated HCl, dried at 60 °C, and packed into tin capsules (Costech Analytical Technologies, Inc.) for elemental analysis on a Elementar Vario EL Cube or Micro Cube elemental analyzer (Elementar Analysensysteme GmbH, Hanau, Germany) interfaced to a PDZ Europa 20–20 isotope ratio mass spectrometer (Sercon Ltd., Cheshire, UK). Peach leaves and glutamic acid were used as calibration standards. The samples were collected primarily in shallow and/or coastal waters, increasing the likelihood of a significant terrestrial source of P (as PIP) or resuspended bottom sediments (Lin et al., 2012). Thus, both PIP and TPP were measured using a modified Aspila et al. (1976) method. Standard reference materials of tomato leaves (NIST #1573a) and estuarine sediment (NIST 1646a) were included in each run to monitor extraction efficiency. POP was then calculated as the difference between TPP and PIP.

Nutrient samples were unfiltered and were analyzed on a segmented continuous flow autoanalyzer (AA3, Seal Analytical) within an hour of collection. $NO_3^- + NO_2^-$ concentrations were determined using a modification of the method outlined in Armstrong et al. (1967). The samples were first passed through a cadmium reduction column to quantitatively reduce the NO_3^- to NO_2^-. The same analysis was performed on the NO_2^- samples, but without the cadmium reduction step. NO_3^- concentrations were then calculated using the following equation: $[NO_3^-] = [NO_3^- + NO_2^-] - [NO_2^-]$. NH_4^+ concentrations were determined fluorometrically according to Kerouel and Aminot (1997). PO_4^{3-} concentrations were measured using the ammonium molybdate method described in Bernhardt and Wilhelms (1967). $Si(OH)_4$ concentrations were determined using the Armstrong et al. (1967) method. It should be noted that all nutrients were measured on unfiltered seawater, which can influence measured concentrations when particulate loads are high due to release of the nutrients within

the particles. For the most part, surface nutrients were depleted, indicating that our sampling was after the major growth season and consequently particulate loads were low.

Water column nutrient stocks were determined by integrating nutrient concentrations down to a depth of 100 m (where appropriate) using the trapezoidal method. Additionally, the water column depth-weighted average concentration of the dissolved inorganic nitrogen (DIN, i.e., the sum of NO_3^-, NO_2^-, and NH_4^+) and PO_4^{3-} was determined at each station.

2.4. Nutrient deficit calculations

The NO_3^- and PO_4^{3-} deficits were determined as the difference between the depth-integrated NO_3^- and PO_4^{3-} concentrations at the start of the growing season (i.e., before the spring/summer phytoplankton bloom) and the concentrations at the time of sampling. All nutrient concentrations were corrected for salinity modification due to ice melt using an upper halocline salinity of 33.1 (Bates and Mathis, 2009). Water column NO_3^- and PO_4^{3-} concentrations at the start of the growing season (i.e., prior to the spring bloom) were assumed equal to the mean concentration in the winter water (WW) we measured on the Chukchi shelf (Fig. 2, Table 1). WW was defined as having a temperature of ≤ -1.6 °C and a NO_3^- concentration of >10 μM (2010 $n=17$ stations, 2011 $n=40$ station) (Fig. 2). This latter constraint is consistent with NO_3^- concentrations in the Chukchi Sea measured in May (pre-phytoplankton bloom) during the Western Arctic Shelf–Basin Interaction program (Codispoti et al., 2005). It also excluded near-surface ice melt waters with temperatures ≤ -1.6 °C. The initial (start of the season) NO_3^- and PO_4^{3-} concentrations at each station were obtained by integrating the mean WW concentrations over the depth of the water column at each station (to a maximum of 100 m). The WW concentrations measured here are consistent with those reported in Codispoti et al. (2005) and new data we collected during May–June, 2014 (unpublished).

The ratio of the NO_3^- and PO_4^{3-} deficits at each station is assumed to be a measure of the phytoplankton NO_3^-:PO_4^{3-} uptake ratio. We also determined the NO_3^-:PO_4^{3-} drawdown ratio for the entire study region, as well as for ACW and BSW, by regressing the measured concentrations of NO_3^- against PO_4^{3-} concentrations. This assumes the in situ concentrations represent the nutrients left over after phytoplankton consumption and that the slope of the resulting line is the phytoplankton NO_3^-:PO_4^{3-} drawdown ratio (sensu Arrigo et al., 1999).

2.5. Excess N calculations

In order to assess the effects of phytoplankton nutrient uptake on excess N concentrations (e.g., N^{**}), and thus on geochemical estimates of denitrification on the Chukchi Shelf, excess N was calculated using two different methods. Method 1 assumed that phytoplankton utilized inorganic N and P according to Redfield stoichiometry. Eq. (1) was altered by removing the constant 2.9 and is referred to here as N^{**}:

$$N^{**} = \left([DIN] - r_{N:P} \times \left[PO_4^{3-}\right]\right), \quad (2)$$

Eq. (2) is similar to that presented in Mordy et al. (2010), although without the regionally determined constant of 5.9. Method 2 assumed that phytoplankton utilized inorganic N and P in non-Redfield (NR) proportions and was calculated as

$$N^{**}_{NR} = \left([DIN] - r_{PON:POP} \times \left[PO_4^{3-}\right]\right), \quad (3)$$

where $r_{PON:POP}$ equals the average PON:POP ratio for each year of the ICESCAPE field campaign. The term excess N is used throughout when referring to the N excess or deficit (i.e., independent of the phytoplankton nutrient utilization ratio used). We use N^{**} and N^{**}_{NR} when differentiating between excess N calculated using the Redfield N:P ratio and the measured (non-Redfield) N:P stoichiometry, respectively.

Table 1
Mean (±SD) and maximum WW NO_3^-, TDIN, and PO_4^{3-} concentrations measured during the ICESCAPE campaign.

	2010			2011		
	Mean ± SD	Max.	n	Mean ± SD	Max	n
NO_3^- (μM)	12.2 ± 1.29	14.9	58	15.5 ± 2.63	20.3	125
TDIN (μM)	14.0 ± 1.51	18.6	58	17.1 ± 2.91	22.2	125
PO_4^{3-} (μM)	1.8 ± 0.17	2.2	58	2.1 ± 0.22	2.5	125

3. Results

3.1. ACC waters

In each of the transects that extended to the Alaskan coast, ACC waters were defined as having a temperature >2 °C and a northward flow. During 2010, Chl *a* concentrations in the ACC (Fig. 3B) surface waters (<10 m) remained low (<1 mg m^{-3}) between the Bering Strait and Barrow Canyon, while subsurface concentrations were generally elevated (>1–8 mg m^{-3}). Subsurface Chl *a* concentrations were highest (~6–8 mg m^{-3}) at 68–71 °N with concentrations decreasing again toward Barrow Canyon. Only PON concentrations decreased along the south to north transit of the ACC during 2010, while both POC and PON concentrations decreased along this same transect in 2011 (Fig. 4A and C, Table 2). In contrast, POP concentrations varied throughout the water column along the path of the ACC; however, there was no discernible south to north pattern during either year (Fig. 4B and D, Table 2).

Nutrient concentrations over the eastern Chukchi Shelf in 2010 were variable, which was likely a consequence of the source water coming through the Bering Strait (i.e., ACW or BSW), and the amount of time light levels were sufficient for phytoplankton growth. DIN concentrations in the surface waters (≤10 m) of the ACC were low, with NO_3^-, NH_4^+, and NO_2^- all <0.1 mmol m^{-3} (Fig. 3C–E). In contrast, surface PO_4^{3-} concentrations were higher and averaged (±SD) 0.5 ± 0.06 mmol m^{-3} (Fig. 3F). At depths >20 m, concentrations of NO_3^-, NO_2^-, and PO_4^{3-} increased along the northward path of the ACC, peaking at locations on the shelf where WW from the BSW (Fig. 1) likely mixed with ACC waters (~159–164°W). NH_4^+ concentrations below 20 m along the ACC were more variable, with the highest concentrations coinciding with peak NO_3^-, NO_2^-, and PO_4^{3-} concentrations, decreasing northward into Barrow Canyon. Nutrient distributions were similar during 2011 (data not shown).

3.2. Non-ACC waters

We used stations in the middle flow path along the Central Channel (Fig. 1) as representative of non-ACC waters on the Chukchi Shelf. These stations contained BSW that flowed northward through the Central Channel and moved cyclonically around Hanna Shoal. They were identified using the hydrographic and ADCP data as those with northward flowing WW and temperatures <2 °C. As noted above, some water from the western flow branch joins the BSW near 72°N. In general, Chl *a* concentrations in these non-ACC waters (Fig. 5B and H) were higher in 2010 than in 2011, with more pronounced subsurface Chl *a* maxima (SCM). Chl *a* concentrations were similar throughout the water column at our western Bering

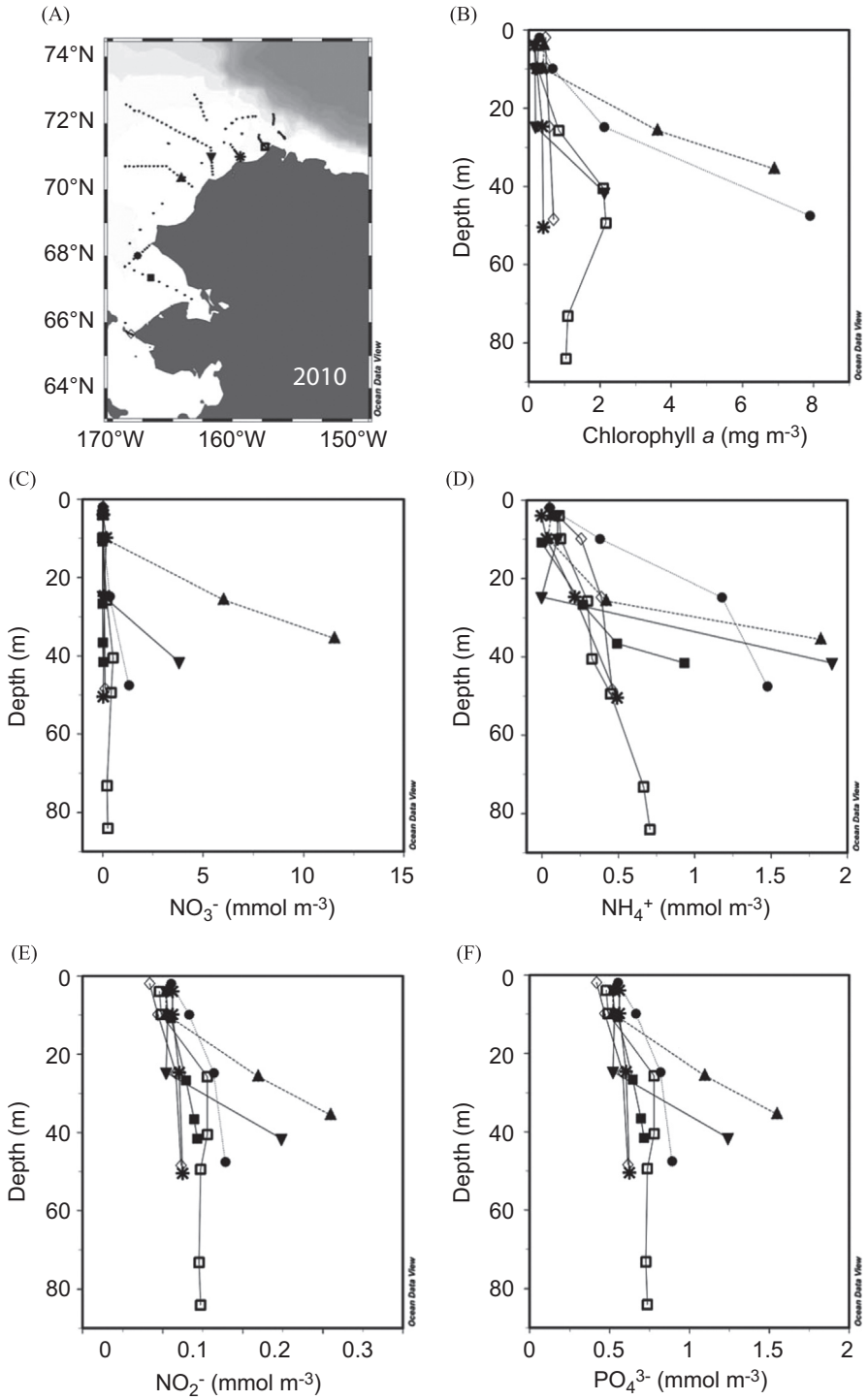

Fig. 3. Profiles of representative ACC stations (A) showing chlorophyll *a* (B), NO_3^- (C), NH_4^+ (D), NO_2^- (E), and PO_4^{3-} concentrations measured during the 2010 ICESCAPE cruise.

Strait sites, although they were much higher in 2010 (~20 mg Chl *a* m^{-3}) than in 2011 (< 2 mg Chl *a* m^{-3}). Chl *a* concentrations in the top 10 m increased as waters advected northward to ~67°N. In fact, the highest concentrations (~50 mg Chl *a* m^{-3}) measured during the 2010 cruise were recorded at 10 m at this site (Fig. 5B). Concentrations at deeper depths were similar to those in the Bering Strait during 2010, but were extremely high in 2011 (> 30 mg Chl *a* m^{-3} at 43 m, Fig. 5H). Further north along the path of the BSW, surface Chl *a* remained below 3 mg m^{-3} during both years. Extremely well developed SCM (≥ 20 mg Chl *a* m^{-3}) were observed at northern stations along the path during 2010, with the exception of the most northeastern site to the east of Hanna Shoal where concentrations in the SCM were below 10 mg Chl *a* m^{-3}. In contrast, during the 2011 season, most northern Chukchi Shelf stations along the BSW flow path had a weaker SCM (< 15 mg Chl *a* m^{-3}), if present. No south to north pattern in the concentrations of POC, PON, or POP were observed in the northward flowing BSW for either year (Fig. 4E–H, Table 2).

Nutrient concentrations in the non-ACC waters of the Bering Strait during both years were vertically well mixed (Fig. 5C–F and I–L). NO_3^- averaged 2.7 ± 0.57 mmol m^{-3} and NO_2^- was 0.04 ± 0.01 mmol m^{-3} during both years. NH_4^+ averaged 1.3 ± 0.14 and

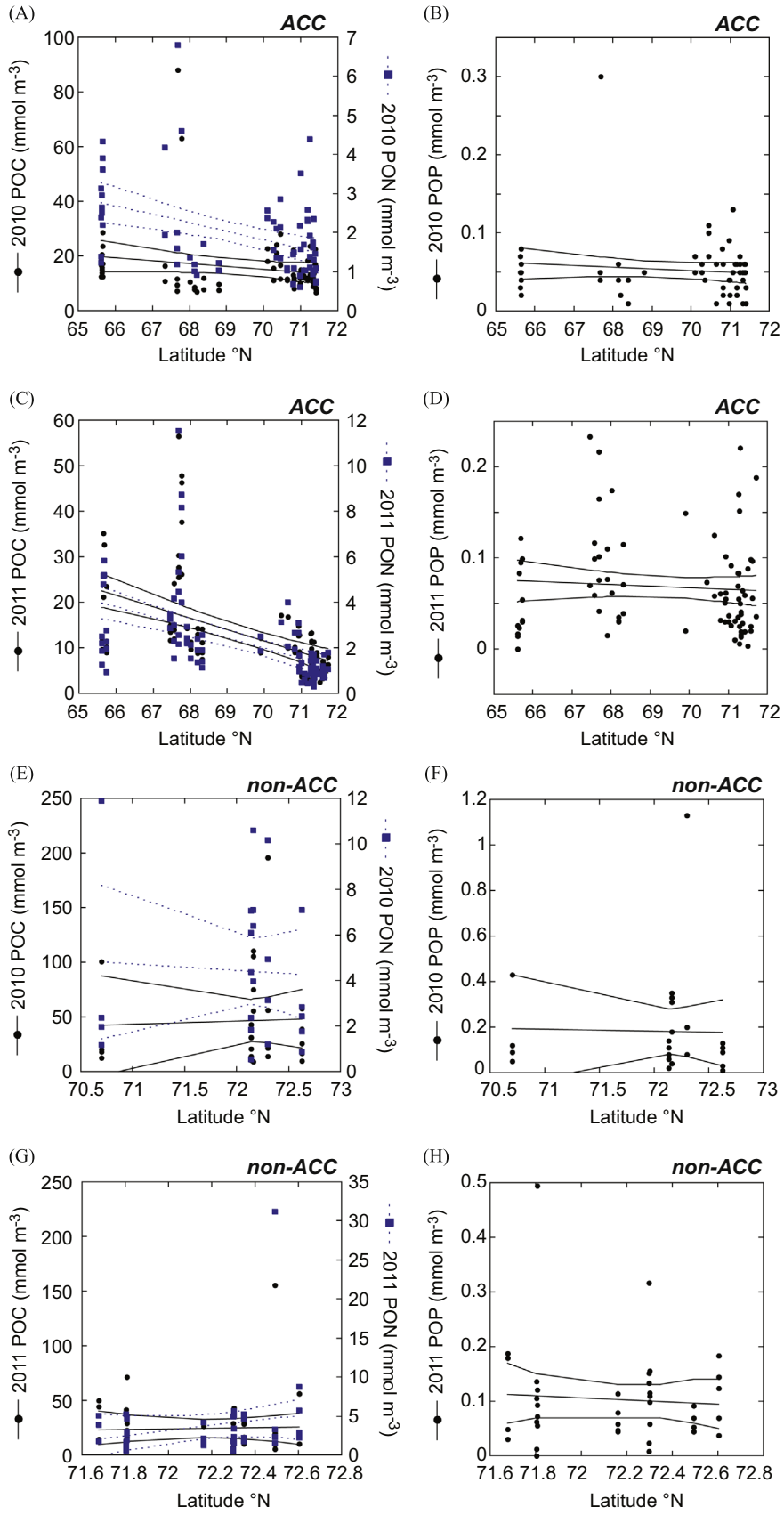

Fig. 4. Latitudinal changes in POC, PON, and POP in ACC (A–D) and non-ACC (E–H) waters during the 2010 (A and B, E and F) and 2011 (C and D, G and H) ICESCAPE cruises. Lines shown are the best-fit linear regressions and their 95% confidence envelopes.

Table 2
Statistics of best-fit linear regressions of changes in POC, PON and POP concentrations in the northward flowing ACC and non-ACC (BSW) waters (data from Fig. 4). Bold indicates statistically significant ($p \leq 0.05$) trends.

	n	Slope	Intercept	R^2	d.f.	MSE	*P*-value
ACC Waters							
2010 POC (mmol m^{-3})	69	−1.05 (0.66)	88.6 (45.9)	0.04	68	340.9	0.12
2010 PON (mmol m^{-3})	69	−0.22 (0.06)	17.1 (4.1)	0.17	68	14.8	**<0.01**
2010 POP (mmol m^{-3})	62	−0.002 (0.002)	0.20 (0.17)	0.01	61	0.001	0.41
2011 POC (mmol m^{-3})	91	−2.53 (0.43)	188.6 (29.5)	0.29	90	2589	**<0.01**
2011 PON (mmol m^{-3})	90	−0.46 (0.08)	34.0 (5.6)	0.52	89	84.1	**<0.01**
2011 POP (mmol m^{-3})	80	−0.002 (0.003)	0.19 (0.19)	0.01	79	0.001	0.52
Non-ACC Waters							
2010 POC (mmol m^{-3})	24	3.04 (14.94)	−172.8 (1076.3)	0.04	23	85.9	0.84
2010 PON (mmol m^{-3})	23	−0.27 (1.11)	23.9 (80.0)	0.05	22	0.68	0.81
2010 POP (mmol m^{-3})	23	−0.01 (0.08)	0.78 (5.71)	0.001	22	0.001	0.92
2011 POC (mmol m^{-3})	42	−0.76 (13.11)	78.9 (945.9)	0.01	41	2.25	0.95
2011 PON (mmol m^{-3})	42	2.29 (2.38)	−161.3 (171.6)	0.02	41	20.6	0.34
2011 POP (mmol m^{-3})	38	−0.02 (0.05)	1.44 (3.36)	0.004	37	0.001	0.69

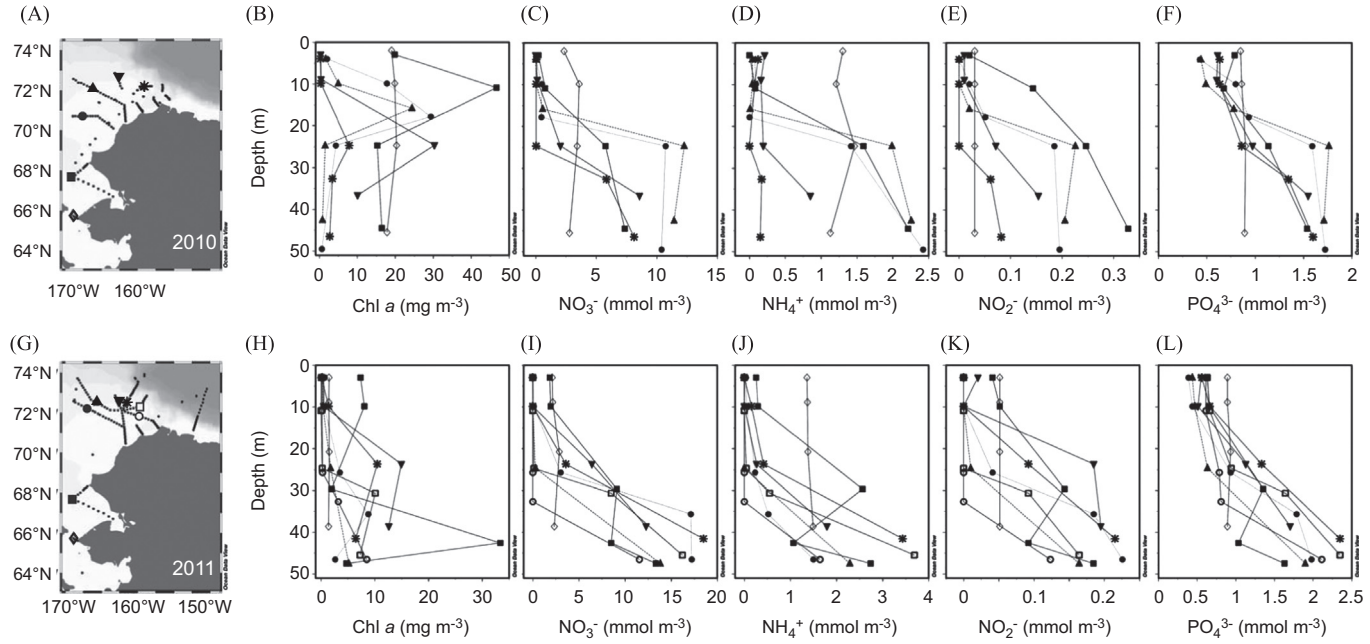

Fig. 5. Profiles of representative western Chukchi Shelf stations (A, G) showing chorophyll *a* (B, H), NO_3^- (C, I), NH_4^+ (D, J), NO_2^- (E, K), and PO_4^{3-} (F, L) concentrations measured during ICESCAPE in both 2010 and 2011.

1.0 ± 0.35 mmol m^{-3} in 2010 and 2011, respectively, while PO_4^{3-} averaged 0.9 ± 0.02 mmol m^{-3} during the two years. Moving north from the Bering Strait along the BSW flow path (Figs. 1 and 5A and G) to stations at 67.7°N, surface depletion of NO_3^- was clearly visible in 2010, while little change in surface concentrations was observed relative to the Bering Strait stations in 2011 (Fig. 5C and I). During both years, NO_3^- concentrations in waters below 20 m at this site were 2–3 fold greater than concentrations farther to the south in Bering Strait. Surface concentrations of NH_4^+ (0.1–0.5 mmol m^{-3}) and PO_4^{3-} (0.5 mmol m^{-3}) were lower relative to surface concentrations in the Bering Strait but higher at depth (NH_4^+ ~2.1–2.8 mmol m^{-3}, PO_4^{3-} = 1.5–1.7 mmol m^{-3}) during both years, while NO_2^- only increased at depth (Fig. 5D–F and J–L). Moving northward along the BSW flow path, DIN concentrations were generally depleted in surface waters over the Chukchi shelf during both 2010 and 2011, although NH_4^+ (in 2010) and NO_2^- (in 2010 and 2011) were slightly elevated in surface waters near ~72 °N (Fig. 5D, E, and K). Over this same area, surface PO_4^{3-} concentrations decreased relative to the Bering Strait, but remained > 0.5 mmol m^{-3}. Below 25 m, nutrient concentrations were enhanced in the non-ACC waters of the northern Chukchi Shelf relative to waters in the Bering Strait (NO_3^- > 5 mmol m^{-3}, NH_4^+ > 1.5 mmol m^{-3}, NO_2^- > 0.1 mmol m^{-3}, and PO_4^{3-} > 1 mmol m^{-3}), although some variability was observed, particularly to the east of Hanna Shoal.

Using the average advective speed of the BSW, nutrients can be plotted as a function of time since the water flowed through the Bering Strait (see Brown et al. (2015) for details on the methodology). In 2010, the rate of decrease (0.14 ± 0.036 mmol m^{-3} d^{-1}) in the mean depth-weighted concentration of DIN ($NO_3^- + NO_2^- + NH_4^+$) along this flow path was significant (Fig. 6 and Table 3), whereas the mean depth-weighted concentration of PO_4^{3-} was not significant. In contrast, both water column integrated DIN and PO_4^{3-} concentrations decreased significantly in 2010 at rates of 7.8 ± 1.76 and 0.4 ± 0.21 mmol m^{-2} d^{-1}, respectively (Fig. 6B, Table 3). No significant decreases in either the depth-weighted mean or depth-integrated concentrations of DIN and PO_4^{3-} were observed in 2011 (Fig. 6C and D, Table 3).

3.3. Nutrient and particulate ratios

The NO_3^-:PO_4^{3-} drawdown ratio (determined from the slope of the best fit line of NO_3^- concentrations regressed against

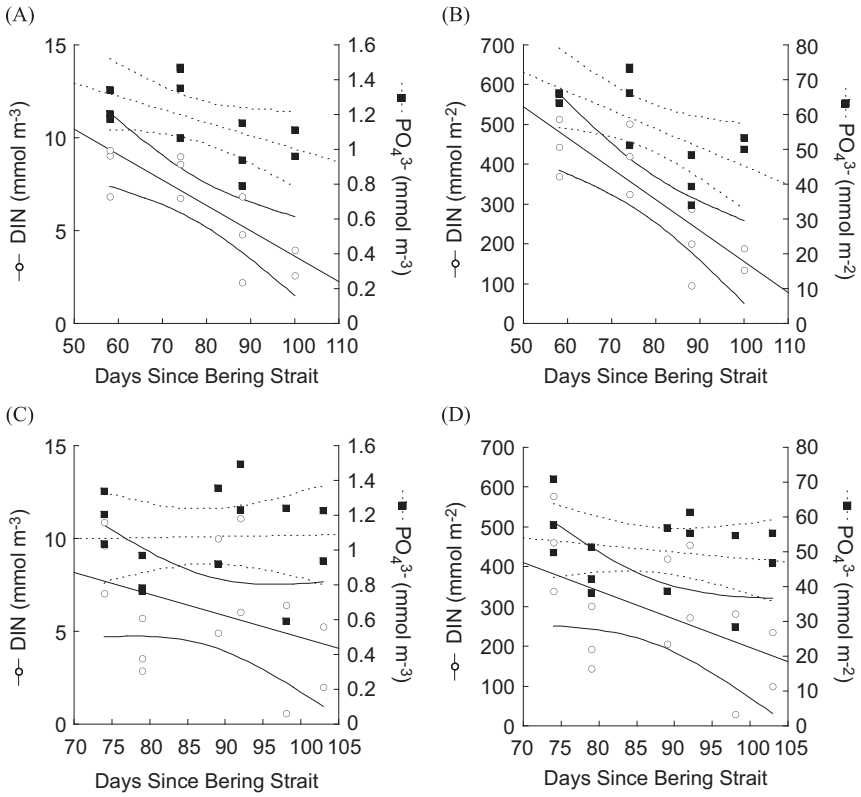

Fig. 6. Change in the mean depth-weighted DIN and PO_4^{3-} concentrations (A, C) and the water column integrated DIN and PO_4^{3-} (B, D) at stations containing WW along the Central Channel BSW flow path during 2010 (A, B) and 2011 (C, D). The *x*-axis shows the elapsed time since waters of each station flowed through Bering Strait, as estimated using the ADCP data. Lines shown are the best-fit linear regressions and their 95% confidence envelopes. Statistics of best-fit regressions are presented in Table 3.

Table 3
Statistics of best-fit linear regressions of changes in mean depth-weighted, integrated and bottom water DIN and PO_4^{3-} concentrations in the northward flowing non-ACC (BSW) waters. Bold indicates statistically significant ($p \leq 0.05$) trends.

	n	Slope	Intercept	R^2	d.f.	MSE	*P*-value
2010 Mean depth-weighted DIN (mmol m^{-3})	12	−0.137 (0.036)	17.3 (2.87)	0.59	11	47.3	**0.004**
2010 Mean depth-weighted PO_4^{3-} (mmol m^{-3})	12	−0.008 (0.0037)	1.76 (0.029)	0.29	11	0.14	0.07
2011 Mean depth-weighted DIN (mmol m^{-3})	14	−0.117 (0.0082)	16.4 (7.21)	0.15	13	20.8	0.18
2011 Mean depth-weighted PO_4^{3-} (mmol m^{-3})	14	0.001 (0.0007)	1.02 (0.615)	< 0.01	13	0.0005	0.93
2010 Integrated DIN (mmol m^{-2})	12	−7.77 (1.758)	932.3 (139.18)	0.66	11	152,900	**0.02**
2010 Integrated PO_4^{3-} (mmol m^{-2})	12	−0.44 (0.208)	98.8 (16.48)	0.40	11	729.7	**0.03**
2011 Integrated DIN (mmol m^{-2})	14	−7.12 (3.543)	908.6 (311.70)	0.25	11	76,490	0.07
2011 Integrated PO_4^{3-} (mmol m^{-2})	14	−0.203 (0.2868)	68.3 (25.23)	0.04	11	62.1	0.49
2010 Mean depth-weighted N^{**} (mmol m^{-3})	12	0.037 (0.072)	−2.09 (5.737)	0.03	11	3.38	0.63
2010 Mean depth-weighted N_{NR}^{**} (mmol m^{-3})	12	−0.015 (0.077)	10.33 (6.116)	< 0.01	11	0.58	0.85
2011 Mean depth-weighted N^{**} (mmol m^{-3})	14	−0.174 (0.024)	2.00 (2.08)	0.82	13	45.70	< **0.001**
2011 Mean depth-weighted N_{NR}^{**} (mmol m^{-3})	14	−0.124 (0.040)	10.46 (3.49)	0.45	13	23.28	**0.009**
2010 Bottom water N^{**} (mmol m^{-3})	11	−0.05 (0.029)	−11.54 (2. 318)	0.21	11	5.89	0.13
2010 Bottom water N_{NR}^{**} (mmol m^{-3})	11	−0.057 (0.027)	0.398 (2.107)	0.31	11	8.16	**0.05**
2011 Bottom water N^{**} (mmol m^{-3})	14	−0.21 (0.033)	2.96 (2.94)	0.77	13	66.28	< **0.001**
2011 Bottom water N_{NR}^{**} (mmol m^{-3})	14	−0.09 (0.058)	10.83 (5.14)	0.17	13	12.3	**0.15**

PO_4^{3-} concentrations in the upper 100 m) for all Chukchi shelf data was less than Redfield proportions in both 2010 (9.0) and 2011 (10.1) (Fig. 7A and C). For both years, the calculated ratio increased slightly when the total DIN pool was used instead of only NO_3^- (10.1 and 11.4 for 2010 and 2011, respectively) (Fig. 7B and D). When separated into ACC stations and central Chukchi Shelf stations, the NO_3^-:PO_4^{3-} drawdown ratios remained well below Redfield stoichiometry in both 2010 and 2011 (Fig. 7). Little difference in NO_3^-:PO_4^{3-} drawdown ratios were observed between ACC and BSW waters (Fig. 7). There was a small increase in slopes ($\leq 7\%$) when stations having NO_3^- concentration below detection limits were excluded from the analysis.

The PON:TPP ratios were lower than Redfield proportions during both 2010 and 2011 with values of 11.8 and 8.6, respectively (Fig. 8A and C). When only organic P was considered (i.e., PON:POP), the ratios were higher. In 2010, PON:POP was 17.2 (Fig. 8B), while in 2011 the PON:POP values were 11.6 (Fig. 8D). The lower PON:TPP values were the result of a high particulate inorganic P fraction. PON:POP ratios were lower in BSW waters than in ACC waters during both years (2010: 9.5 and 16.2, respectively; 2011: 6.8 and 13.1, respectively).

3.4. Nutrient deficits

Depth-integrated nutrient deficits relative to WW values over the ICESCAPE study area ranged 7.5-fold during 2010, with the

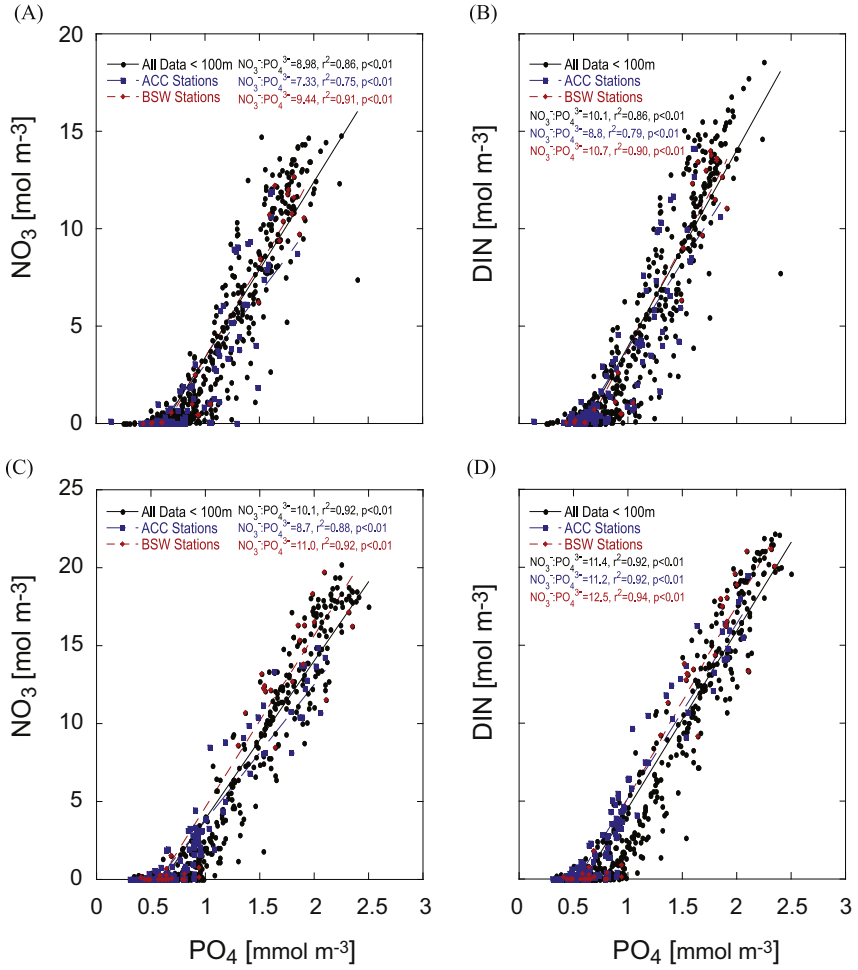

Fig. 7. NO_3^- to PO_4^{3-} (A, C) and DIN to PO_4^{3-} (B, D) relationships of all ICSCAPE data combined (black), at ACC stations (blue), and at BSW stations (red) during 2010 and 2011. The inset ratio represents the seasonal phytoplankton drawdown ratio of either NO_3^-:PO_4^{3-} or DIN: PO_4^{3-}. Lines show the best-fit linear regressions for each data set. (For interpretation of the references to color in this figure legend, the reader is referred to the web version of this article.)

NO_3^- deficit averaging 588 ± 250 mmol m^{-2} and the PO_4^{3-} deficit averaging 63 ± 25 mmol m^{-2} (Fig. 9A and B). In 2011, deficits were higher and varied even more (~14 fold) with NO_3^- and PO_4^{3-} deficits averaging 930 ± 450 and 82 ± 38 mmol m^{-2}, respectively (Fig. 9D and E). Deficits were small in the northwest portion of our study area and in the region of Kotzebue Sound (66°N, 163°W), while the maximum deficits were located near 68°N (in 2011) and in Barrow Canyon (both years). Deficits detected in the non-ACC waters over the Chukchi Shelf in 2010 (NO_3^-: 397 ± 104 mmol m^{-2}, PO_4^{3-}: 43 ± 11 mmol m^{-2}) were smaller than those measured during 2011 (NO_3^-: 633 ± 167 mmol m^{-2}, PO_4^{3-}: 57 ± 14 mmol m^{-2}). The ACC is a summertime water mass and thus the deficits calculated for these waters (along the coast) are not reliable.

Over the majority of the Chukchi Sea, the ratio of the NO_3^- deficit to the PO_4^{3-} deficit (NO_{3def}^-:$PO_{4\,def}^{3-}$) was well below Redfield stoichiometry, averaging 9.2 ± 0.9 and 11.2 ± 1.2 in 2010 and 2011, respectively (Fig. 9C and F). The minimum $NO_{3\,def}^-$:$PO_{4\,def}^{3-}$ corresponded to regions on the shelf within the BSW (Fig. 1). Curiously, the maximum $NO_{3\,def}^-$:$PO_{4\,def}^{3-}$ (~18) was located to the northwest in the region of a large under-ice phytoplankton bloom (Arrigo et al., 2012). These waters likely received input of non-shelf waters via wind driven upwelling (Spall et al., 2014) that influenced the nutrient inventory in this region and thus impacted deficit estimates.

3.5. Excess nitrogen (N^{**} and N_{NR}^{**})

The mean depth-weighted excess N ranged by up to 4-fold over the entire Chukchi Shelf (Fig. 10) and differed dramatically between N^{**} (Fig. 10A and C) and N_{NR}^{**} (Fig. 10B and D). N^{**} (determined using Redfield N:P proportions) averaged -2.4 ± 5.9 mmol m^{-3} and -12.6 ± 2.4 mmol m^{-3} in 2010 and 2011, respectively, indicating a large deficit of NO_3^- relative to PO_4^{3-}. Values for N_{NR}^{**} (determined using measured particulate N:P proportions) were much higher, averaging 4.1 ± 7.1 mmol m^{-3} in 2010 and -1.9 ± 2.3 mmol m^{-3} in 2011. The difference between the two mean depth-weighted excess N calculations over the entire study area was 6.5 ± 2.0 mmol m^{-3} in 2010 (Fig. 11A) and 10.8 ± 3.4 mmol m^{-3} in 2011 (Fig. 11B).

There was a noticeable change in N^{**} as potential density decreased. Between σ_θ of ~25 and 28 kg m^{-3}, N^{**} was variable, ranging between -22.0 and -6.0 mmol m^{-3} (mean-$= -12.9 \pm 3.3$ mmol m^{-3}, Fig. 12A). At potential densities ≤ 24 kg m^{-3}, N^{**} was higher (-11.4 ± 1.3 mmol m^{-3}, avg $\pm$ s.d.) and less variable (–13.3 to –6.8 mmol m^{-3}). The lower excess N values at higher potential densities were reversed when calculated as N_{NR}^{**}. Potential densities >25 kg m^{-3} averaged -1.5 ± 3.5 mmol m^{-3}, while densities ≤ 24 kg m^{-3} were smaller and less variable averaging -5.9 ± 2.9 mmol m^{-3} (Fig 12B). These relationships suggest that there is a relationship between N^{**} and depth. This is evident for the upper 50 m where N^{**} decreased significantly with

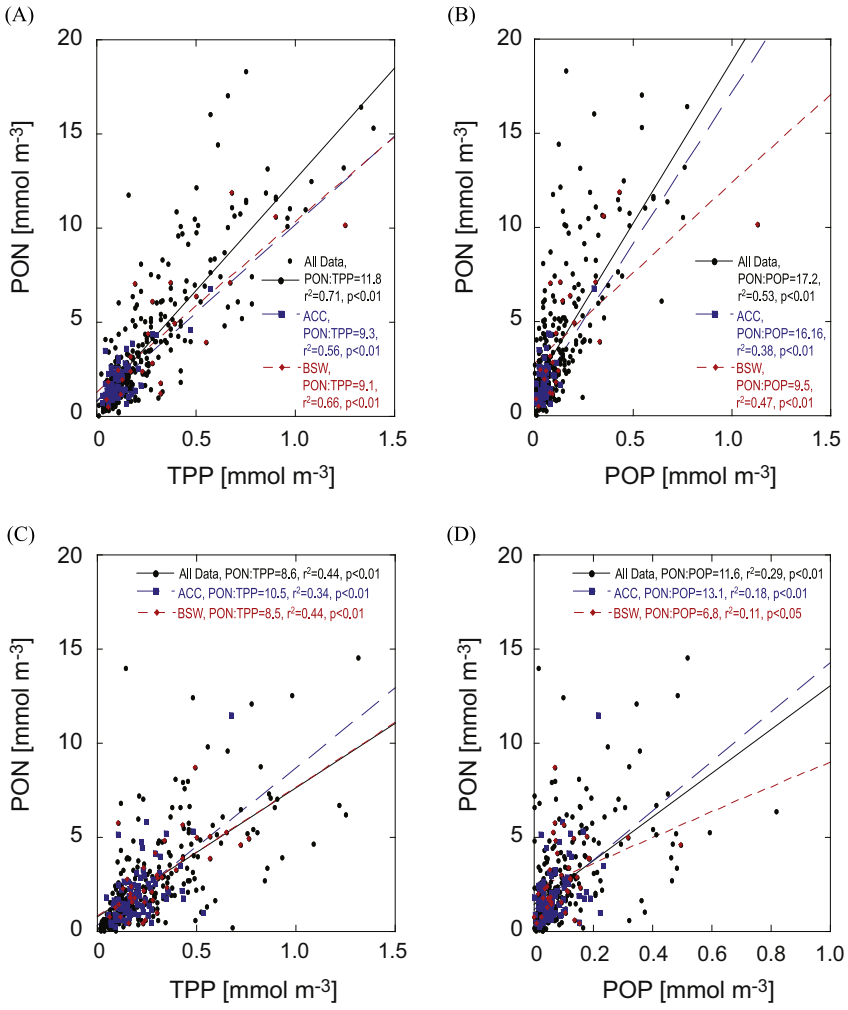

Fig. 8. The PON to POP (A, C) and PON to POP relationships of all ICSCAPE data combined (black), at ACC stations (blue), and at BSW stations (red) during 2010 and 2011. The inset ratio shows the PON:TPP or PON:POP ratio for each data set. Lines show the best-fit linear regressions for each data set. (For interpretation of the references to color in this figure legend, the reader is referred to the web version of this article.)

increasing depth (Fig. 12C). Below 50 m, there was no significant relationship between N^{**} and depth. No significant relationship between N^{**}_{NR} and depth in the upper 50 m (Fig. 12D) was detected either.

Excess N concentrations varied along the BSW flow path from the Bering Strait northwards toward Barrow Canyon. This is clearly seen when the concentration of excess N at stations with WW located along this flow path are plotted as a function of the number of days since the water at each station was in Bering Strait (Fig. 13). The mean depth-weighted water column N^{**} increased slightly along this flow path in 2010, while the mean depth-weighted N^{**}_{NR} showed no change (Fig. 13A). In contrast, both N^{**} and N^{**}_{NR} decreased as water flowed northward across the Chukchi Shelf in 2011. The rate of decrease was -0.17 ± 0.02 mmol m^{-3} d^{-1} for N^{**} and a lower rate of -0.12 ± 0.04 mmol m^{-3} d^{-1} for N^{**}_{NR} (Fig. 13A and B, Table 3). When only the bottom 10 m of the water column was analyzed for changes in excess N along the flow path of BSW on the Chukchi Shelf, a significant decrease was observed in both years. In 2010, there was little difference in the rate of decrease when bottom water excess N was calculated using Redfield or non-Redfield proportions ($N^{**} = -0.5 \pm 0.03$ vs. $N^{**}_{NR} = -0.6 \pm 0.03$ mmol m^{-3} d^{-1}) (Fig. 13C, Table 3). In 2011 though, bottom water concentrations of N^{**} decreased three times faster than N^{**}_{NR} (-0.21 ± 0.03 vs. -0.09 ± 0.06 mmol m^{-3} d^{-1}) (Fig. 13D) along the flow path of BSW.

The rate of decrease of excess N along the BSW flow path is presumably the result of N loss due to sedimentary denitrification and can therefore be used to estimate denitrification rates. Multiplying the rates of excess N decrease from Table 3 (slopes in Fig. 13A–D) by either the average water column depth (49 ± 3.9 m) along the BSW flow path or the thickness of the bottom WW layer (10 m) (Brown et al., 2015) provides an areal rate of denitrification (Table 4). Denitrification rates determined using the bottom waters were higher in 2011 than in 2010. There was no decrease in the mean depth weighted N^{**} as water flowed northward across the shelf in 2010, and thus comparison of the two years was not possible. Daily rates of denitrification over the Chukchi Shelf estimated from N^{**}_{NR} were approximately equal to (in 2010 bottom waters) or less than the N^{**} determined rates (both depth-weighted and bottom water in 2011). In 2011, daily rates of denitrification determined from N^{**}_{NR} were 43–70% of the rates determined from N^{**} (Table 4). Applying these rates across the whole shelf area of the Chukchi Sea sampled during ICESCAPE (5.41×10^5 km^2) results in annual denitrification rates of 16.3 and 23.0 Tg N yr^{-1}, respectively, when mean depth-weighted N^{**}_{NR} and N^{**} measures of excess N concentrations are used. When integrated only over the bottom 10 m, annual shelf denitrification rates were 75% lower for N^{**} and 85% lower for N^{**}_{NR} in 2011 (5.8 and 2.5 Tg N yr^{-1}, respectively, Table 4). During 2010, the estimated annual rates of denitrifcation in the bottom 10 m were lower, with the N^{**}_{NR} calculated rates slightly higher than the N^{**}determined rates (1.7 and 1.4 Tg N yr^{-1}, respectively, Table 4) (Fig. 13).

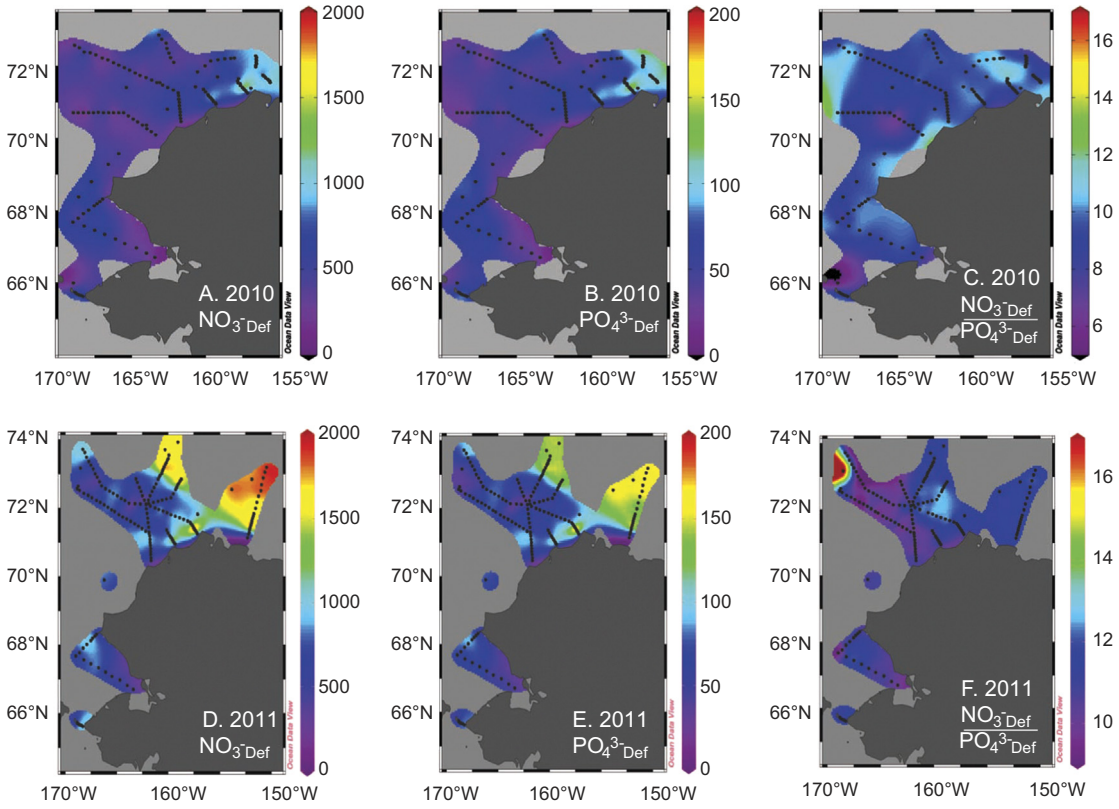

Fig. 9. The NO_3^- (A, D) and PO_4^{3-} (B, E) deficits (mmol m^{-2}) and the $NO_3^-{}_{DEF}$:$PO_4^{3-}{}_{DEF}$ deficit ratios (C, F) integrated over the top 100 m in the Chukchi Sea during 2010 (A–C) and 2011 (D–F).

4. Discussion

4.1. Phytoplankton N:P ratios

The fact that phytoplankton stoichiometry can deviate from Redfield proportions is well established (Arrigo et al., 1999; Geider and La Roche, 2002) and was even acknowledged by Redfield (1958). The plasticity in phytoplankton N:P ratios partly results from cellular adjustments to environmental conditions. Individual phytoplankton cells can change their cellular composition in response to changes in the organism's physical (light, temperature) or chemical (nutrient concentration, salinity) surroundings. Under optimal conditions (e.g., nutrient and light replete), cells may enhance their growth potential by increasing concentrations of macromolecules such as ribosomal RNA and nucleic acids that have a relatively low N:P ratio (Elser et al., 1996). Under growth-limiting conditions, cellular constituents are shifted toward macromolecules involved in resource acquisition, such as photosynthetic pigments and nutrient uptake proteins, which have relatively high N:P ratios. In agreement with this, a recent global survey of particulate elemental stoichiometry showed latitudinal patterns of phytoplankton with lower than Redfield stoichiometry in nutrient rich high latitude regions and higher than Redfield stoichiometry in the nutrient depleted oceanic gyres (Martiny et al., 2013). The relationship between growth rate on the one hand, and the dependence of cellular stoichiometry on the macromolecular composition on the other, is referred to as "the growth rate hypothesis" (GRH) (Sterner and Elser, 2002).

The ICESCAPE data presented here support the ubiquity of non-Redfield stoichiometry in marine systems. We provide evidence that consumption of inorganic NO_3^- and PO_4^{3-} by phytoplankton in the Chukchi Sea is at a ratio of 11.4 ± 3.04 (all data combined), significantly less than the canonical Redfield ratio of 16:1. Our data are consistent with previous studies from the Arctic showing lower than Redfield nutrient uptake by phytoplankton. Harrison et al. (1982) found N:P assimilation ratios of 6:1 in the eastern Canadian Arctic waters of Baffin Bay, while Tamelander et al. (2012) documented lower than Redfield stoichiometry of suspended particles in the Fram Strait. Additionally, low NO_3^-:PO_4^{3-} utilization by Arctic phytoplankton was observed in the Beaufort Sea (Bergeron and Tremblay, 2014) and in the northern Chukchi Sea (~12) (Tremblay, pers. comm., 2013). Furthermore, similarly low N:P drawdown ratios were recorded in the Bering Sea by Horak et al. (2013).

The PON:POP ratios were, for the most part, low as well (Fig. 8). The only exception was in 2010 (Fig. 8b). The higher than Redfield values were recorded primarily in ACC waters, while lower than Redfield values were observed in the BSW waters. Phytoplankton particulate N:P ratios are influenced by both species composition and growth conditions. The Chukchi Sea phytoplankton communities during the ICESCAPE campaign were overwhelmingly dominated by diatoms (Laney and Sosik, 2014), which are from the red algal superfamily and believed to have evolved low N:P stoichiometry (Quigg et al., 2003). That diatoms have a low N:P utilization ratio is supported by multiple field investigations (Arrigo et al., 1999; Moore et al., 2007; Hauss et al., 2012).

PO_4^{3-} concentrations during ICESCAPE were never depleted. Under P-replete conditions, phytoplankton can accumulate P beyond what is needed for growth and store it as polyphosphate (luxury uptake) (Diaz et al., 2008), and thus lower their N:P ratio. Evidence shows that some diatoms can increase allocation of cellular P to polyphosphates under P deficient conditions (Perry, 1976; Dyhrman et al., 2012) which may result in sustained low particulate N:P ratios under these conditions.

In addition, nutrient concentrations are believed to affect phytoplankton N:P ratios by impacting growth rates and cellular macromolecular content (Geider and La Roche 2002; Klausmeier et al., 2004;

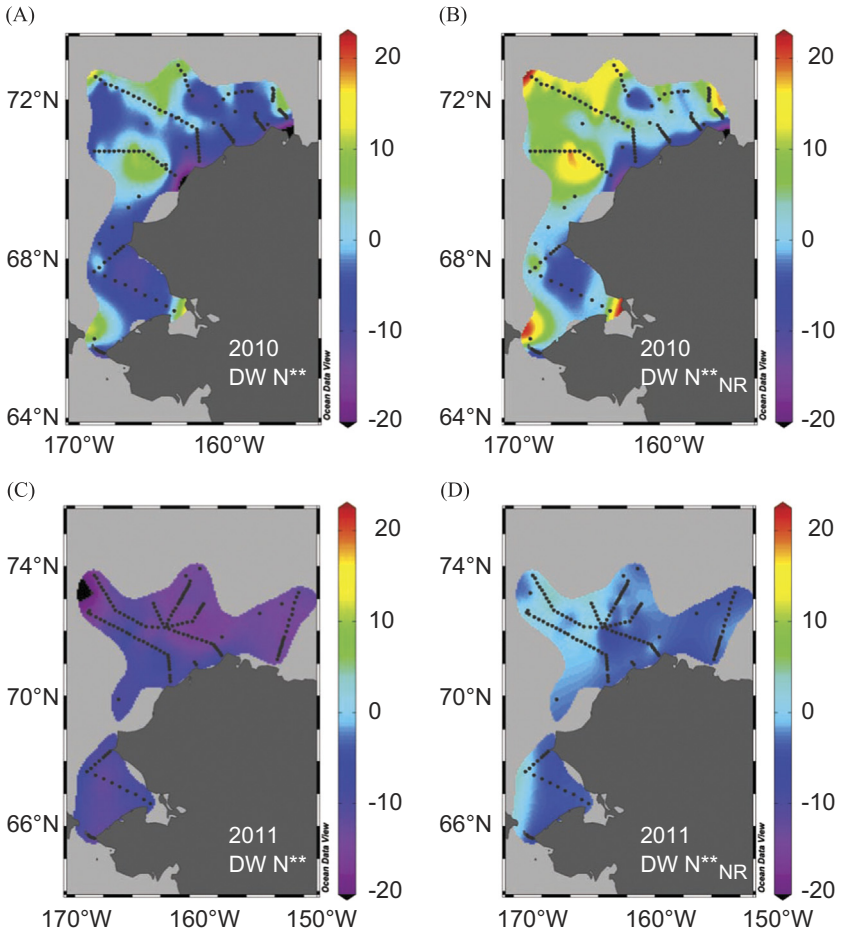

Fig. 10. Mean depth weighted (DW) excess N concentrations (mmol m^{-3}) calculated as N^{**} (A, D) or N^{**}_{NR} (B, E).

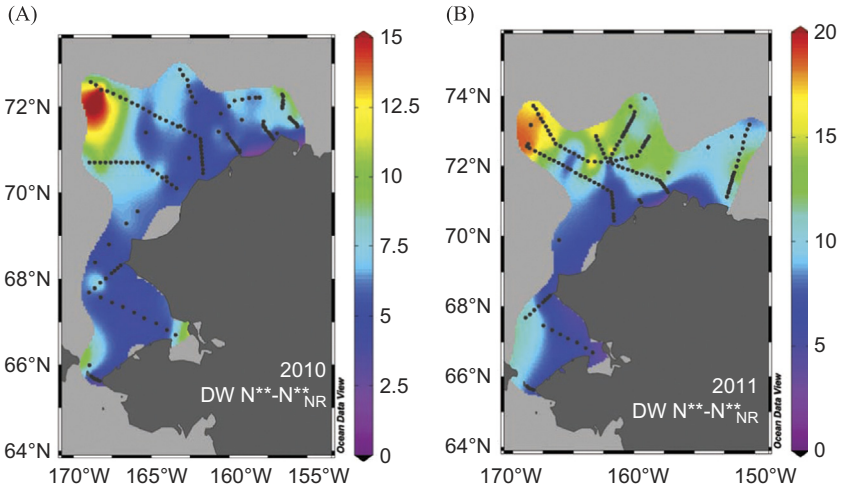

Fig. 11. Difference between the mean depth weighted (DW) excess N concentrations in 2010 (A) and 2011 (B).

Arrigo, 2005). Under non-nutrient limited growth conditions, phytoplankton are believed to have a macromolecular composition with a lower N:P content (i.e., low protein:rRNA ratio) and thus a low cellular N:P content. Under nutrient limited growth, the protein:rRNA content is expected to increase, thereby increasing the cellular N:P content.

The waters throughout the Chukchi Shelf during our cruise were deficient in dissolved N relative to dissolved P, with DIN being mostly undetectable in surface waters, and thus phytoplankton were likely N-limited during our study. The PON:POP ratios can indicate the growth conditions during the time of sampling (i.e., a high PON:POP ratio may indicate a slow phytoplankton growth rate and suggest that the surface waters were deficient in dissolved N), NO_3^-:PO_4^{3-} drawdown ratios represent nutrient consumption over the productive season when nutrients were replete. Thus, the low phytoplankton NO_3^-:PO_4^{3-} utilization ratios we detected are consistent with non-Redfield proportion nutrient utilization. During the nutrient-limited summer season, the NO_3^-:PO_4^{3-} ratio was likely higher, as the high PON:POP content of the 2010 ACC samples suggest. These samples

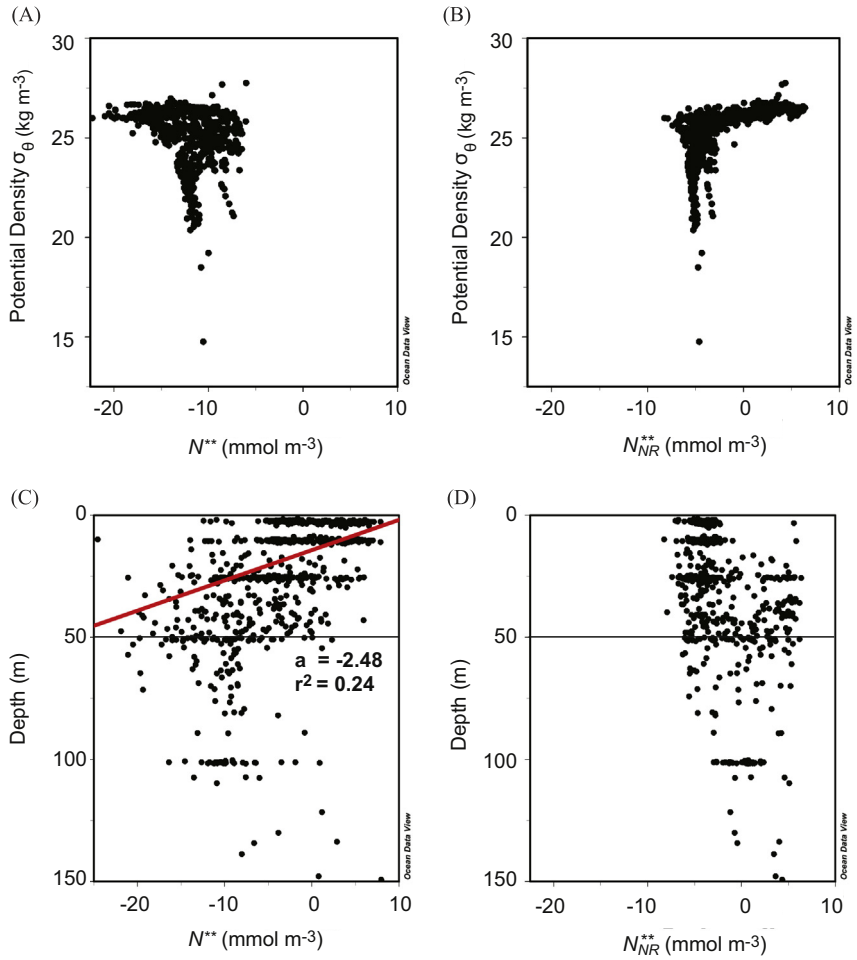

Fig. 12. Relationships between potential density (σ_0) and N^{**} (A) or N^{**}_{NR} (B) and depth and N^{**} (C) or N^{**}_{NR} (D) during 2011. Shown in (C) is the best-fit linear regressions between excess N and depth in the upper 50 m. The corresponding slope and regression coefficient are also reported.

were collected later in the year than the 2011 samples, and were thus obtained from the most nutrient-depleted waters.

4.2. Deficits and productivity estimates

The nutrient deficits measured during the ICESCAPE campaign ranged 7–14 fold over the area we sampled on the Chukchi Shelf, with high deficits recorded in waters to the north of the shelf-break. These calculated deficits in the Canada Basin north of the shelf are likely overestimates due to our assumption that winter-time NO_3^- values are equal to those on the shelf. In the oligotrophic basin waters, NO_3^- concentrations are low year round (Codispoti et al., 2013), and we do not have reliable data for winter water NO_3^- concentrations in these waters. Additionally, nutrient deficits in the ACC are difficult to assess due to the fact that it is a summertime water mass formed from coastal runoff in the Gulf of Alaska and the Bering Sea. As such, the nutrient deficits calculated there using Chukchi Shelf WW nutrient concentrations are likely inaccurate, and thus difficult to interpret. We therefore consider only Chukchi shelf waters (those <150 m) for the remainder of the nutrient deficit discussion.

Nutrient deficits were highest on the shelf near 68°N 169°W (during 2010) and in Barrow Canyon (both years). High consumption of NO_3^- in and around Barrow Canyon is not surprising as this region is widely recognized for its high productivity (Hill and Cota, 2005; Grebmeier, 2012; Bates and Mathis, 2009). Furthermore, in the ICESCAPE field years, the sea ice retreated earlier at both of these locations than on other parts of the shelf, allowing a longer time for nutrient deficits to develop (Lowry et al., 2014). Ice typically retreats early on the northeast Chukchi Shelf due to the arrival of the warm ACC waters (e.g., Weingartner et al., 1998), and, in some years, due to easterly winds that open up polynyas in the region (e.g., Itoh et al., 2012). This exposes the northeastern Chukchi Sea to solar radiation relatively early in the season. In contrast, much of the northwestern portion of our study site was ice covered during ICESCAPE.

Hansell et al. (1993) estimated maximum NO_3^- deficits of $\sim$800 mg-at NO_3^- N m^{-2} (1 mg-at NO_3^- N = 1 mmol NO_3^- m^{-3}) on the southern portion of the Chukchi shelf near 68°N, 169°W. Our calculated maximum NO_3^- deficits were of similar magnitude (2010: 580 ± 110 mmol NO_3^- m^{-2} and 2011: 785 ± 127 mmol NO_3^- m^{-2}) in this region. The Barrow Canyon NO_3^- deficits were higher, averaging 906 ± 191 mmol NO_3^- m^{-2} in 2010 and 1173 ± 410 mmol NO_3^- m^{-2} in 2011. Hansell et al. (1993) did not present nutrient deficits north of $\sim$68°N so our values cannot be directly compared for this region.

The seasonal consumption of NO_3^- can be used to estimate new production on the Chukchi shelf. Converting the NO_3^- deficits to equivalent C units using the C:N values from ICESCAPE (all values ≤ 150 m, 2010 C:N = 8.4 ± 0.3, 2011 C:N = 5.7 ± 0.1, Mean $\pm$ SE) results in new production estimates near 68°N that averaged 70 ± 14 and 74 ± 11 g C m^{-2} in 2010 and 2011, respectively. These are consistent with the value of $\sim$70 g C m^{-2} estimated by Hansell et al. (1993) for the Chukchi Shelf between 64° and 68°N. Our estimates of new production are even higher

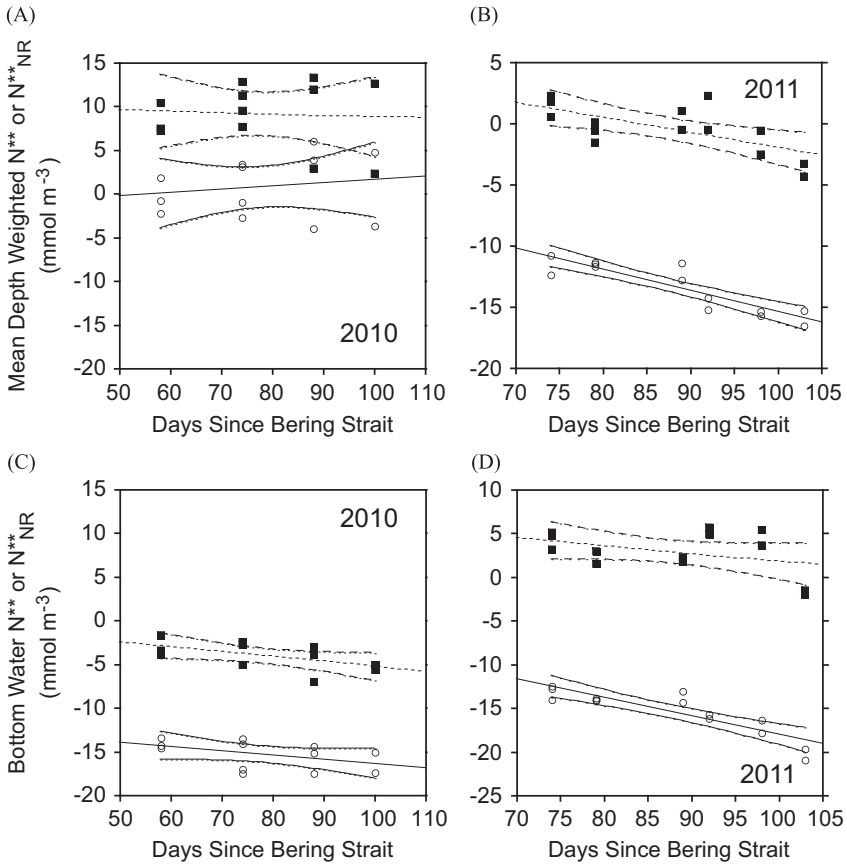

Fig. 13. Change in excess N concentrations as water flowed along the Central Channel during 2010 (A, C) and 2011 (B, D). Shown are depth weighted average water column excess N concentrations (A, B) or the excess N concentration of only the bottom waters (C, D) along the flow path. Open circles are $N^*$and closed squares are N^*_{NR}. Lines shown are the best-fit linear regressions and their 95% confidence envelopes. Statistics of best-fit regressions are presented in Table 2.

Table 4
Denitrification rate estimates along the Central Channel BSW flow path and over the Chukchi shelf calculated from changes in excess nitrogen concentrations assuming Redfield and non-Redfield stoichiometry.

	Central channel flow path		Chukchi Shelf[a]	Chukchi Shelf[a]	N^{**}_{NR}:N^{**}	Mean:BW
	(mmol N m^{-2} d^{-1}) 2010	(mmol N m^{-2} d^{-1}) 2011	(Tg N yr^{-1}) 2010	(Tg N yr^{-1}) 2011		
Water column depth weighted mean						
N^{**}		8.3		23.0		
N^{**}_{NR}		5.9		16.3	0.7	
Bottom water						
N^{**}	0.5	2.1	1.4	5.8		3.9
N^{**}_{NR}	0.6	0.9	1.7	2.5	0.4–1.2	6.5
Chang and Devol (2008)	0.96		2.7 (4.4)			
Devol et al. (1997)	0.49–2.8		1.4–7.7			

[a] Area of the Chukchi Shelf is 5.41×10^5 km^2, numbers in ( ) are maximums.

in the Barrow Canyon region, averaging 116 ± 25 and 105 ± 37 g C m^{-2} in 2010 and 2011, respectively. These values all fall within the range of 5–160 g C m^{-2} reported for the Chukchi Sea in the review of Arctic productivity by Sakshaug (2004). Codispoti et al. (2013) also calculated new production from nutrient drawdown in the northern and southern Chukchi Sea (termed $NCP\Delta_{nut}$ in their paper), which ranged from 10 to 70 g C m^{-2}. However, they used Redfield C:N (6.6) to convert NO_3^- deficits to carbon equivalents, which are less than we measured in 2010, but higher than our 2011 measured ratios. Higher than Redfield C:N ratios in particulate matter have been measured in the Arctic by several studies (Sambrotto et al., 1993; Walsh et al., 1989). Thus, new production estimates determined by Redfield stoichiometric conversion of NO_3^- deficits likely represent lower bounds. We also note that our estimates account for new production up to the time of sampling (July 21st in 2010 and July 29th in 2011), and are therefore conservative.

Given that new production accounts for 20–50% of total primary production on the Chukchi Shelf (Hansell et al., 1993; Codispoti et al., 2013), our new production estimates convert to a total primary production in our study region ranging between 140 and 680 g C m^{-2} during the growing season. The Sakshaug (2004) estimate of annual primary productivity in the Chukchi Sea (20– > 400 g C m^{-2}) encompasses the lower range of our

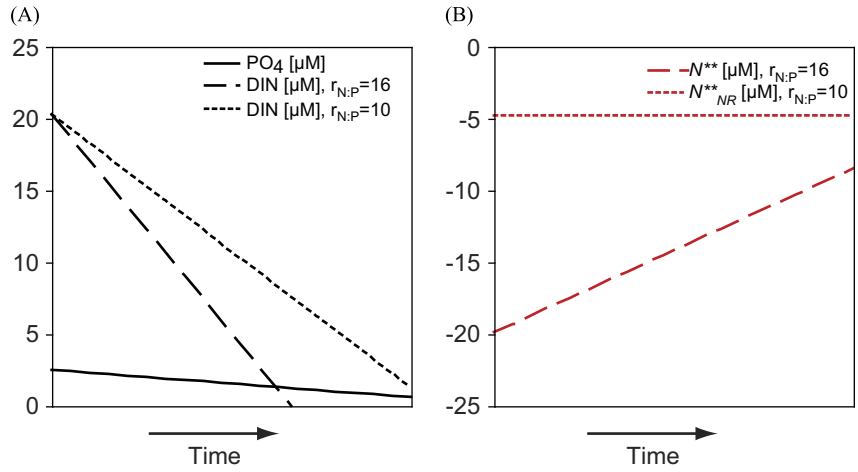

Fig. 14. Schematic showing Redfield and lower than Redfield DIN and PO_4^{3-} consumption (A) and the resulting excess N concentration (N^{**} and N^{**}_{NR})(B). $r_{N:P}$ is the ratio of DIN:PO_4^{3-} consumption.

estimates, while the Hansell et al. (1993) estimate (576–720 g C m^{-2}) brackets the maximum total primary production we calculate. The area of the Chukchi Shelf is approximately 5.41×10^5 km^2, and thus this equates to 75–368 Tg C produced by phytoplankton per growth season in 2010 and 2011 on the Chukchi Shelf; consistent with Codispoti et al. (2013) who estimated primary production on the Chukchi Shelf to be 156 Tg C.

Arrigo and Van Dijken (2011) estimated the mean annual primary production in the Chukchi Sea between 1998 and 2009 to be 29.1 ± 5.3 Tg C yr^{-1} using satellite ocean color data. One limitation of ocean color measurements is that only phytoplankton in the first optical depth in open water are detected. As a result, phytoplankton blooms that occur at deeper depths or the massive under-ice blooms observed in the northeastern area of the ICESCAPE study region, are not detected. Thus, satellite-derived estimates of primary production in seasonally ice-covered regions of the Chukchi Sea may be up to an order of magnitude too low (Arrigo et al., 2012). In contrast, productivity estimates made from nutrient deficits, as in the present study (see also Hansell et al., 1993; Codispoti et al., 2013), are spatially and temporally integrated over the water column and growth season and include any production that takes place in the water column beneath the ice.

4.3. N excess and denitrification

The low DIN:PO_4^{3-} ratios measured in the Pacific Arctic are attributed to sedimentary denitrification (Yamamoto-Kawai et al., 2006); water column denitrification in Arctic waters is negligible due to high O_2 levels (Brown et al., 2015). Direct measurements of denitrification rates in the Arctic range from 0.1 to 2.8 mmol N m^{-2} d^{-1} (Chang and Devol, 2009; Devol et al., 1997), with denitrification in the Chukchi Sea accounting for approximately 23% of the entire Arctic Ocean. As a whole, the Arctic accounts for 4–13% of total global denitrification, which is remarkable considering it accounts for ~4% of global ocean area.

These high rates of denitrification are driven by the high productivity of phytoplankton in the Arctic. The Chukchi Sea is an area of relatively high new production (70–116 g C m^{-2} yr^{-1} estimated here), much of which sinks to the sea floor and provides the organic N that is ultimately released as NH_4^+ via microbial ammonification. Much of this NH_4^+ is then nitrified to NO_2^- and then NO_3^-. Eventually, some of this NO_3^- is denitrified to N_2 (Granger et al., 2011; Brown et al., 2015), which is unavailable for consumption by most bacteria and phytoplankton. In this manner, the Arctic, and in particular the Chukchi Sea, is a significant global sink of fixed N.

In addition, some POP associated with the exported organic matter is eventually remineralized to PO_4^{3-}. Seasonal mixing of the entire water column results in the release of both the regenerated DIN and PO_4^{3-} from the sediments, though the loss of bioavailable N due to denitrification means that the DIN:PO_4^{3-} ratio of the regenerated nutrients is lower than the N:P of the source particulate material. As such, the waters in the Arctic have a low DIN:PO_4^{3-} ratio.

The nutrient tracer N^* (N^{**} here) is used to diagnose the relative importance of denitrification and N fixation on the oceanic N inventory (Gruber and Sarmiento 1997; Deutsch et al., 2001; Codispoti et al., 2005). The high rates of denitrification make the Arctic an oceanic sink for fixed N, as characterized by the low N^{**} measured in this study and by others (e.g., Codispoti et al., 2005, 2009; Kaltin and Anderson, 2005; Nishino et al., 2005). Different formulas for the calculation of excess N have been developed (Gruber and Sarmiento, 1997; Deutsch et al., 2001; Nishino et al., 2008), making comparisons of excess N estimates between studies somewhat difficult. The N^{**} formula used by Codispoti et al. (2005) was different from that used here, employing factors that produced a global excess N average equal to zero and accounted for phosphate released from organic matter during denitrification. The latter constant (0.87), as originally derived by Gruber and Sarmiento (1997) has been demonstrated by Deutsch et al. (2001) to result in underestimates of excess N due to the conversion of fixed N (organic N, NH_4^+, and NO_3^-) to N_2. Additionally we did not employ the first constant (2.98) that sets the excess N global average equal to zero because we constructed our excess N equation using regional data. Taking these differences in formulas into account, our N^{**} concentrations and distributions are consistent with those measured by Codispoti et al. (2005).

Both this study and Codispoti et al. (2005) show that shelf water N^{**} concentrations are generally lower in more dense waters (i.e., N^{**} decreases with depth on the Chukchi Shelf, Fig. 12C). This trend with depth provides further evidence of non-Redfield N and P utilization by phytoplankton. If phytoplankton utilization in surface waters consumes more P than N (relative to the Redfield ratio), the residual nutrient pool will be enriched in N relative to the phytoplankton utilization ratio (i.e., high N^{**}). Deeper in the water column, the remineralization of low N:P organic matter that sinks to the bottom could potentially decrease N^{**} at depth. The net effect of non-Redfield nutrient consumption by phytoplankton and their subsequent remineralization is a decrease in N^{**} with depth, which is clearly seen in the upper 50 m of the Chukchi Shelf (Fig. 12C). Below 50 m though, little change in N^{**} over depth is observed since the majority of nutrient depletion by phytoplankton is in the upper 50 m.

Thus, this change in N^{**} with depth is likely a consequence of the implicit assumption in the definition of N^{**} that phytoplankton utilize nutrients in Redfield proportions (Fig. 14). When Redfield stoichiometry is assumed, but actual phytoplankton utilization ratios are less than Redfield proportions, the excess N concentration increases as nutrients are depleted. However, if the measured phytoplankton nutrient utilization ratio is used when calculating excess N concentrations, then excess N (here N^{**}_{NR}) concentrations remain constant as nutrients are depleted (Fig. 14B). This is illustrated in the ICESCAPE data where surface N^{**} concentrations decrease with depth (i.e., along the gradient of nutrient uptake), and by the lack of change in surface water (<50 m) N^{**}_{NR} concentrations with depth (Fig. 12D). Coincidentally, Horak et al. (2013) measured a positive change in Bering Sea Shelf excess N concentrations during the summer season, which they attribute to low N to P drawdown by summer phytoplankton during the spring bloom.

By removing the imprint of phytoplankton nutrient utilization on excess N, N^{**}_{NR} is a more valid tracer of N cycle sources and sinks than N^{**}. While N fixation has been detected in Arctic waters (Blais et al., 2012), rates are low and the impact on the Arctic N inventory is likely insignificant. We therefore limit our discussion only to denitrification.

An analysis of changes in excess N along the northward flow path of winter water on the Chukchi Shelf reveals different estimates of denitrification rates when N^{**} or N^{**}_{NR} are used. In 2010, denitrification rates calculated from N^{**}_{NR} and N^{**} differed little, but this was not the case for 2011, when rates were 1.4–2.0 times higher when determined using N^{**} than N^{**}_{NR}. In addition, the calculated denitrification rates were higher (1.5–4 times) in 2011 than in 2010. While both campaigns sampled the same area of the Chukchi Shelf, the 2010 expedition was conducted earlier in the season. As such, ice cover was higher and nutrient depletion was less in 2010. Nutrient deficits were greater in 2011, likely the result of higher concentrations in winter water. The higher deficits in 2011 suggest that productivity was also higher that year. Productivity positively correlates with denitrification (Ward, 2013), and thus the higher denitrification rates in 2011 than 2010 are consistent with the yearly differences in nutrient deficits.

Our daily rates of denitrification determined from bottom water N^{**}_{NR} in 2010 are similar to previous average estimates of denitrification (Devol and Christensen, 1993; Chang and Devol, 2009). In contrast, the 2011 denitrification rates determined from changes in mean depth-weighted water column excess N concentrations are much higher (2.1–8.6 fold) than the maximum rates previously measured by Devol and Christensen (1993) or Chang and Devol (2009). Although the daily rates of denitrification calculated here using the mean depth weighted N^{**}_{NR} concentrations are high, they are not unprecedented in continental shelf or coastal regions (see Joye and Anderson (2008)). It should be kept in mind that our estimates of changes in excess N are determined from the total DIN pool. Consequently, other processes that result in loss of DIN, such as anaerobic ammonium oxidation (anammox), which can be significant in the Arctic (Thamdrup and Dalsgaard, 2002; Rysgaard et al., 2004; Gihring et al., 2010), are included in the denitrification estimate. In contrast, the determinations of denitrification in the Chukchi Sea by Devol et al. (1997) and Chang and Devol (2009) are dependent only on changes in NO_3^- and not on other forms of DIN. Likewise, the direct measurements of denitrification presented in Devol et al. (1997) and Chang and Devol (2009) are of a relatively limited spatial and temporal scope. In contrast, the rates estimated here integrate over larger spatial (100s of km) and temporal (3–4 mos.) scales, which may potentially more accurately capture denitrification rates on the Chukchi Shelf. When scaled to the area of the entire Chukchi Shelf we calculate that denitrification accounts for a loss of 2.5 and 16.3 Tg N yr^{-1}, in bottom waters and the depth-weighted water column, respectively. Assuming a global marine denitrification rate of 120–240 Tg N yr^{-1} (DeVries et al., 2013), our estimates suggest that the Chukchi Sea would account for as little as 1% and as much as 13.5% of global marine denitrification.

5. Conclusion

The data presented here suggest that phytoplankton in the Chukchi Sea utilize nutrients (N and P) at less than the Redfield ratio. Thus, estimates of excess N in this region that assume Redfield proportions can overestimate denitrification rates by up to 40%. Taking this into account, we developed the geochemical tracer N^{**}_{NR} to estimate rates of denitrification in the Chukchi Sea. Even with this more accurate method, our rates of denitrification are higher (by up to 8-fold) than previously documented. Given the dependence of denitrification on organic matter production (Ward, 2013), the documented increasing rates of primary productivity with the retreating Arctic ice (Arrigo and van Dijken, 2011), and the significant rates of denitrification presented here for the Chukchi Sea, the Arctic Ocean will likely become a more significant global N sink, playing an increased role in the global N inventory.

Acknowledgements

This work was supported by the Ocean Biology and Biogeochemistry Program and the Cryosphere Science Program of the National Aeronautic and Space Administration under Grant no. NNX10AF42G to KRA and RSP. We also thank the Captain and crew of the USCGC Healy for their help in conducting this research. The authors would also like to acknowledge two anonymous reviewers and the members of the Arrigo Lab at Stanford University for their helpful suggestions that led to the publication of this manuscript.

References

Armstrong, F.A.J., Stearns, C.R., Strickland, J.D.H., 1967. The measurement of upwelling and subsequent biological processes by means of the Technicon AutoAnalyzer™ and associated equipment. Deep-Sea Res. 14 (3), 381–389.

Arrigo, K.R., Robinson, D.H., Worthen, D.L., Dunbar, R.B., DiTullio, G.R., VanWoert, M., Lizotte, M.P., 1999. Phytoplankton community structure and the drawdown of nutrients and CO_2 in the Southern Ocean. Science 283 (5400), 365–367.

Arrigo, K.R., 2005. Marine microorganisms and global nutrient cycles. Nature 437 (7057), 349–355.

Arrigo, K.R., Van Dijken, G.L., 2011. Secular trends in Arctic Ocean net primary production. J. Geophys. Res. 116 (C09011).

Arrigo, K.R., Perovich, D.K., Pickart, R.S., Brown, Z.W., Van Dijken, G.L., Lowry, K.E., Mills, M.M., Palmer, M.A., Balch, W.M., Bahr, F., Bates, N.R., Benitez-Nelson, C., Bowler, B., Brownlee, E., Ehn, J.K., Frey, K.E., Garley, R., Laney, S.R., Lubelczyk, L., Mathis, J., Matsuoka, A., Mitchell, B.G., Moore, G.W.K., Ortega-Retuerta, E., Pal, S., Polashenski, C.M., Reynolds, R.A., Schieber, B., Sosik, H.M., Stephens, M., Swift, J.H., 2012. Massive phytoplankton blooms under the Arctic sea ice. Science 336, 1408.

Aspila, K.I., Agemian, H., Chau, A.S.Y., 1976. A semi-automated method for the determination of inorganic, organic, and total phosphorus in sediments. Analyst 101, 187–197.

Bates, N.R., Mathis, J.T., 2009. The Arctic ocean marine carbon cycle: evaluation of air–sea CO_2 exchanges, ocean acidification, and potential feedbacks. Biogeosciences 6, 2433–2459.

Bergeron, M., Tremblay, J.-É., 2014. Shifts in biological productivity inferred from nutrient drawdown in the southern Beaufort Sea (2003–2011) and northern Baffin Bay (1997–2011), Canadian Arctic. Geophys. Res. Lett. 41, 3979–3987. http://dx.doi.org/10.1002/2014GL059649.

Bernhardt, H., Wilhelms, A., 1967. The continuous determination of low level iron, soluble phosphate and total phosphate with the AutoAnalyzer ™. Technicon Symp. 1 (386), 385–389.

Blais, M., Tremblay, J.E., Jungblut, A.D., Gagnon, J., Martin, J., Thaler, M., Lovejoy, C., 2012. Nitrogen fixation and identification of potential diazotrophs in the Canadian Arctic. Global Biogeochem. Cycles 26 (GB3022), http://dx.doi.org/10.1029/2011GB004096.

Brown, Z.W., Cascioti, K.L., Pickart, R.S., Swift, J.H., Arrigo, K.R., 2015. Aspects of the marine nitrogen cycle of the Chukchi Sea shelf and Canada Basin. Deep-Sea Res. II 118 (PA), 73–87. http://dx.doi.org/10.1016/j.dsr2.2015.02.009.

Chang, B.X., Devol, A.H., 2009. Seasonal and spatial patterns of sedimentary denitrification rates in the Chukchi Sea. Deep-Sea Res. II 56, 1339–1350.

Codispoti, L.A., Flagg, C., Kelly, V., Swift, J.H., 2005. Hydrographic conditions during the 2002 SBI process experiments. Deep Sea Res. II 52, 1144–1163.

Codispoti, L.A., Flagg, C., Swift, J.H., 2009. Hydrographic conditions during the 2004 SBI process experiments. Deep Sea Res. II 56, 1144–1163.
Codispoti, L.A., Kelly, V., Thessen, A., Matrai, P., Suttles, S., Hill, V., Steele, M., Light, B., 2013. Synthesis of primary production in the Arctic Ocean: III. Nitrate and phosphate based estimates of net community production. Prog. Oceanogr. 110, 107–125.
Deutsch, C., Gruber, N., Key, R.M., Sarmiento, J.L., Ganachaud, A., 2001. Denitrification and N_2 fixation in the Pacific Ocean. Global Biogeochem. Cycles 15 (2), 483–506.
Devol, A.H., Christensen, J.P., 1993. Benthic fluxes and nitrogen cycling in sediments of the continental-margin of the eastern North Pacific. Journal of Marine Research 51 (2), 345–372.
Devol, A.H., Codispoti, L.A., Christensen, J.P., 1997. Summer and winter denitrification rates in western Arctic shelf sediments. Cont. Shelf Res. 17, 1029–1050.
DeVries, T., Deutsch, C., Rafter, P.A., Primeau, F., 2013. Marine Denitrification Rates Determined from a Global 3-D Inverse Model.
Diaz, J., Ingall, E., Benitez-Nelson, C., Patterson, D., De Jonge, M.D., McNulty, I., Brandes, J.A., 2008. Marie polyphosphate: a key player in geologic phosphorus sequestration. Science 320, 652–655.
Dyhrman, S.T., Jenkins, B.D., Rynearson, T.A., Saito, M.A., Mercier, M.L., Alexander, H., Whitney, L.P., Drzewianowski, A., Bulygin, V.V., Bertrand, E.M., Wu, Z., Benitez-Nelson, C., Heithoff, A., 2012. The transcriptome and proteome of the Diatom *Thalassiosira pseudonana* reveal a diverse phosphorus stress response. PLoS One 7 (3), e33768. http://dx.doi.org/10.1371/journal.pone.0033768.
Elser, J.J., Dobberfuhl, D.R., MacKay, N.A., Schampel, J.H., 1996. Organism size, life history, and N:P stoichiometry: toward a unified view of cellular and ecosystem processes. Bioscience 46, 674–684.
Geider, R.J., La Roche, J., 2002. Redfield revisited: variability of C:N:P in marine microalgae and its biochemical basis. Eur. J. Phycol. 37 (1), 1–17.
Gihring, T.M., Lavik, G., Kuypers, M.M.M., Kostka, J.E., 2010. Direct determination of nitrogen cycling rates and pathways in Arctic fjord sediments (Svalbard, Norway). Limnol. Oceanogr. 55, 740–752.
Granger, J.M., Prokopenko, M.J., Sigman, D.M., Mordy, C.W., Morse, Z.M., Morales, L. V., Sambrotto, R.N., Plessen, B., 2011. Coupled nitrification-denitrification in sediment of the eastern Bering Sea shelf leads to (^{15}N) N enrichment of fixed N in shelf waters. J. Geophys. Res. 116 (C11006), http://dx.doi.org/10.1029/2010JC006751).
Grebmeier, J.M., 2012. Shifting patterns of life in the Pacific Arctic and sub-Arctic seas. Annu. Rev. Mar. Sci. 4, 63–78.
Gruber, N., Sarmiento, J.L., 1997. Global patterns of marine nitrogen fixation and denitrification. Global Biogeochem. Cycles 11 (2), 235–266.
Gruber, N., 2008. The marine nitrogen cycle: overview of distributions and processes. In: Capone, D.G., Bronk, D.A., Mulholland, M.R., Carpenter, E.J. (Eds.), Nitrogen in the Marine Environment. Elsevier, Amsterdam, pp. 1–50.
Hansell, D.A., Whitledge, T., Goering, J.J., 1993. Patterns of nitrate utilization and new production over the Bering–Chukchi shelf. Cont. Shelf Res. 13, 601–627.
Harrison, W.G., Platt, T., Irwin, B., 1982. Primary production and nutrient assimilation by natural phytoplankton populations of the Eastern Canadian Arctic. Can. J. Fish. Aquat. Sci. 39 (2), 335–345.
Hauss, H., Franz, J.M.S., Sommer, U., 2012. Changes in N:P stoichiometry influence taxanomic composition and nutritional quality of phytoplankton in the Peruvian upwelling. J. Sea Res. 73, 74–85.
Hill, V., Cota, G., 2005. Spatial patterns of primary production on the shelf, slope and basin of the Western Arctic in 2002. Deep Sea Res. II 52, 3344–3354.
Holm-Hansen, O., Lorenzen, C.J., Holmes, R.W., Strickland, J.D.H., 1965. Fluormetric determination of Chlorophyll. ICES J. Mar. Sci. 30 (1), 3–15.
Horak, R.E.A., Whitney, H., Shull, D.H., Mordy, C.W., Devol, A.H., 2013. The role of sediments on the Bering Sea shelf N cycle: Insights from measurements of benthic denitrification and benthic DIN fluxes. Deep Sea Res. II 94, 95–105.
Itoh, M., Shimada, K., Kamoshida, T., McLaughlin, F., Carmack, E., Nishino, S., 2012. Interannual variability of Pacific Winter Water inflow through Barrow Canyon from 2000 to 2006. J. Oceanogr. 68, 575–592.
Joye, S.B., Anderson, I.C., 2008. Nitrogen cycling in estuarine and nearshore sediment. In: Capone, D.G., Bronk, D.A., Carpenter, E.J., Mullhollond, M. (Eds.), Nitrogen in the Marine Environment. Springer-Verlag, pp. 868–915.
Kaltin, S., Anderson, L.G., 2005. Uptake of atmospheric carbon dioxide in Arctic shelf seas: evaluation of the relative importance of processes that influence pCO_2 in water transported over the Bering–Chukchi shelf. Mar. Chem. 94, 67–79.
Kerouel, R., Aminot, A., 1997. A fluorometric determination of ammonia in seas and estuarine waters by direct segmented flow analysis. Mar. Chem. 57, 265–275.
Lin, P., Guo, L., Chen, M., Tong, J., Lin, F., 2012. The distribution and chemical speciation of dissolved and particulate phosphorus in the Bering Sea and the Chukchi–Beaufort Seas. Deep Sea Res. II—Top. Stud. Oceanogr. 81–84, 79–94.
Klausmeier, C.A., Litchman, E., Daufresne, T., Levin, S.A., 2004. Optimal nitrogen-to-phosphorus stoichiometry of phytoplankton. Nature 429 (6988), 171–174.
Laney, S.R., Sosik, H.M., 2014. Phytoplankton assemblage structure in and around a massive under-ice bloom in the Chukchi Sea. Deep Sea Res. II—Top. Stud. Oceanogr. 105, 30–41.
Lowry, K.E., VanDijken, G.L., Arrigo, K.R., 2014. Evidence of under-ice phytoplankton blooms in the Chukchi Sea from 1998 to 2012. Deep Sea Res. II—Top. Stud. Oceanogr. 105, 105–117.
Martiny, A.C., Pham, C.T.A., Primeau, F.W., Vrugt, J.A., Moore, J.K., Levin, S.A., Lomas, M.W., 2013. Strong latitudinal patterns in the elemental ratiosof marine planktob and organic matter. Nature Groscience 6, 279–283.
Mills, M.M., Arrigo, K.R., 2010. Magnitude of oceanic nitrogen fixation influenced by the nutrient uptake ratio of phytoplankton. Nat. Geosci. 3 (6), 412–416.
Moore, C.M., Seeyave, S., Hickman, A.E., Allen, J.T., Lucas, M.I., Planquette, H., Pollard, R.T., Poulton, A.J., 2007. Iron-light interactions during the CROZet natural iron bloom and EXport experiment (CROZEX) I: phytoplankton growth and photophysiology. Deep Sea Res. II—Top. Stud. Oceanogr. 54 (18–20), 2045–2065.
Mordy, C.W., Eisner, L.B., Proctor, P., Stabeno, P., Devol, A.H., Shull, D.H., Napp, J.M., Whitledge, T., 2010. Temporary uncoupling of the marine nitrogen cycle: accumulation of nitrite on the Bering Sea shelf. Mar. Chem. 121, 157–166.
Nishino, S., Shimada, K., Itoh, M., 2005. Use of ammonium and other nitrogen tracers to investigate the spreading of shelf waters in the western Arctic halocline. J. Geophys. Res. 110, http://dx.doi.org/10.1029/2003JC002118.
Nishino, S., Shimada, K., Itoh, M., Yamamoto-Kawai, M., Chiba, S., 2008. East-west differences in water mass, nutrient, and chlorophyll a distributions in the sea ice reduction region of the western Arctic Ocean. J. Geophys. Res. 113, http://dx.doi.org/10.1029/2007JC004666.
Pabi, S., van Dijken, G.L., Arrigo, K.R., 2008. Primary production in the Arctic Ocean, 1998–2006. J. Geophys. Res.—Oceans 113, C08005. http://dx.doi.org/10.1029/2007JC004578.
Padman, L., Erofeeva, S., 2004. A barotropic inverse tidal model for the Arctic Ocean. Geophys. Res. Lett. 31, http://dx.doi.org/10.1029/2003GL019003.
Perry, M.J., 1976. Phosphate utilization by an oceanic diatom in phosphorus-limited chemostat culture and in oligotrophic waters of central north-Pacific. Limnol. Oceanogr. 21 (1), 88–107.
Pickart, R.S., Pratt, L.J., Torres, D.J., Whitledge, T.E., Proshutinsky, Y., Aagaard, K., Agnew, A., Moore, G.W.K., Dail, H.J., 2010. Evolution and dynamics of the flow through Herald Canyon in the Western Chukchi Sea. Deep Sea Res. II 57, 5–26.
Quigg, A., Finkel, Z.V., Irwin, A.J., Rosenthal, Y., Ho, T.Y., Reinfelder, J.R., Schofield, O., Morel, F.M.M., Falkowski, P.G., 2003. The evolutionary inheritance of elemental stoichiometry in marine phytoplankton. Nature 425 (6955), 291–294.
Quigg, A., Irwin, A.J., Finkel, Z.V., 2011. Evolutionary inheritance of elemental stoichiometry in phytoplankton. Proc. R. Soc. Lond. B 278, 526–534.
Redfield, A.C., 1958. The biological control of chemical factors in the environment. Am. Scientist 46, 205–221.
Rysgaard, S., Glud, R.N., Risgaard-Petersen, N., Dalsgaard, T., 2004. Denitrification and anammox activity in Arctic marine sediments. Limnol. Oceanogr. 49, 1493–1502.
Sakshaug, E., 2004. Primary and secondary production in Arctic seas. In: Stein, R., MacDonald, R.W. (Eds.), The Organic Carbon Cycle in the Arctic Ocean. Springer, New York, pp. 57–81.
Sambrotto, R.N., Savidge, G., Robinson, C., Boyd, P., Takahashi, T., Karl, D.M., Langdon, C., Chipman, D., Marra, J., Codispoti, L.A., 1993. Elevated consumption of carbon relative to nitrogen in the surface ocean. Nat. Geosci. 363, 248–250.
Spall, M.A., 2007. Circulation and water mass transformation in a model of the Chukchi Sea. J. Geophys. Res. 112, C05025. http://dx.doi.org/10.1029/2005JC002264.
Spall, M.A., Pickart, R.S., Brugler, E.T., Moore, G.W.K., Thomas, L., Arrigo, K.R., 2014. Role of shelfbreak upwelling in the formation of a massive under-ice bloom in the Chkchi Sea. Deep Sea Res. II 105, 17–29.
Sterner, R.W., Elser, J.J., 2002. Ecological Stoichiometry: The Biology of Elements from Molecules to the Biosphere. Princeton University Press, Princeton.
Tamelander, T., Aubert, A.B., Riser, C.W., 2012. Export stoichiometry and contribution of copepod fecal pellets to vertical flux of particulate organic carbon, nitrogen, and phosphorus. Mar. Ecol. Prog. Ser. 459, 17–28.
Thamdrup, B., Dalsgaard, T., 2002. Production of N_2 through anaerobic ammonium oxidation coupled to nitrate reduction in marine sediments. Appl. Environ. Microbiol. 68, 1312–1318.
Walsh, J.J., Mcroy, C.P., Coachman, L.K., Goering, J.J., Nihoul, J.J., Whitledge, T.E., Blackburn, T.H., Parker, P.L., Wirick, C.D., Shuert, P.G., Grebmeier, J.M., Springer, A.M., Tripp, R.D., Hansell, D.A., Djenidi, S., Deleersnijder, E., Henriksen, K., Lund, B.A., Andersen, P., Mullerkarger, F.E., Dean, K., 1989. Carbon and nitrogen cycling within the Bering Chukchi Seas—source regions for organic-matter effecting AOU demands of the Arctic-Ocean. Prog. Oceanogr., 22; , pp. 277–359.
Ward, B.B., 2013. How nitrogen is lost. Science 341, 352.
Weingartner, T.J., Aagaard, K., Woodgate, R., Danielson, S., Sasaki, Y., Cavalieri, D.J., 2005. Circulation on the north central Chukchi Sea shelf. Deep Sea Res. II 52, 3150–3174.
Weingartner, T.J., Cavalieri, D.J., Aagaard, K., Sasaki, Y., 1998. Circulation, dense water formation, and outflow on the northeast Chukchi shelf. J. Geophys. Res. 103, http://dx.doi.org/10.1029/1098JC00374.
Yamamoto-Kawai, M., Carmack, E., McLaughlin, F., 2006. Nitrogen balance and Arctic throughflow. Nature 443 (7107), 43.